Title:

A TNL receptor mediates microbiome feedbacks in Arabidopsis

Authors:

Henry Janse van Rensburg[1*], Niklas Schandry[2,3*§], Jan Waelchli[1], Katja Stengele[1], Selma Cadot[1], Katharina Jandrasits[2], Hiroaki Adachi[4,5], Claude Becker[2,3,§], Klaus Schlaeppi[1,§]

[1] Department of Environmental Sciences, University of Basel, Basel, Switzerland

[2] Gregor Mendel Institute of Molecular Plant Biology GmbH, Austrian Academy of Sciences, Vienna BioCenter (VBC), Vienna, Austria

[3] LMU Biocenter, Faculty of Biology, Ludwig-Maximilians-Universität Munich, Martinsried, Germany

[4] Graduate School of Agriculture, Kyoto University, Kyoto, Japan

[5] Faculty of Advanced Life Science, Hokkaido University, Sapporo, Japan

[*] Contributed equally

[§] **Corresponding authors:**

Niklas Schandry: n.schandry@bio.lmu.de

Claude Becker: claude.becker@lmu.de

Klaus Schlaeppi: klaus.schlaeppi@unibas.ch

ORCID identifiers:

H. J.v.R.:	0000-0002-5632-8422
N. S.:	0000-0003-3099-7860
J. W.:	0000-0002-4384-6570
K. St.:	0009-0008-3843-2868
S. C.:	0000-0003-3939-2593
K. J.:	0000-0002-0161-582X
H. A.:	0000-0002-7184-744X
C. B.:	0000-0003-3406-4670
K. S.:	0000-0003-3620-0875

Author contributions:

H.J.v.R., N.S., C.B., and K.S., designed the research; H.J.v.R. and K. St. performed greenhouse and S.C. the field soil conditionings; K.J and N.S. performed the phenotyping of accessions and GWA analysis; H.J.v.R. performed GWA candidate gene selection, MBOA sensitivity assays, genetic characterisation of Arabidopsis mutants, Arabidopsis mutant feedback, microbiome and transcriptome

experiments and analysis; J.W., performed bioinformatic analysis for the microbiome and transcriptome analyses; H.A. performed structural modelling; C.B., provided funding and access to high-throughput phenotyping infrastructure; H.J.v.R. and N.S. analysed the data; H.J.v.R., N.S. and K.S. wrote the manuscript. All authors revised the paper.

Manuscript information:

Number of Figures: 8 (all colour)

Number of Extended Data Figures: 9

Number of Supplementary Materials figures: 2

Number of Supplementary Materials tables: 3

Declarations of interest:

none

Abstract

Plant performance depends on the soil microbiome. While microbiome feedbacks are well documented, the mechanisms by which plants perceive and mediate these feedbacks remain unclear. We established a framework using two distinct microbiomes in the same soil, where one led to enhanced growth of the *Arabidopsis thaliana* accession Col-0. Screening 410 accessions revealed substantial variation in growth feedbacks, which we used for genome-wide association mapping. We identified the immune receptor *Mediator of Microbiome Feedback 1* (*MMF1*) as a candidate gene involved in microbiota feedbacks. Characterisation in the reference accession Col-0 revealed that *mmf1* mutants lost the beneficial growth feedback, had an altered root bacterial community, and failed to induce a defence-related transcriptional response observed in wild-type plants. The discovery of MMF1 implies that integration of microbial signals optimises host microbiome composition and immune status to enhance growth.

Keywords

Growth feedback, GWAS, Arabidopsis, soil microbiome, TNL receptors

Main

Microbiomes are widely recognized for supporting their hosts with many vital services, often leading to improved host performance. Similar to the gut microbiome of humans, plant root microbiomes contribute to nutrition homeostasis, stress tolerance and host health (*1*). For plants, above-ground performance depends to a large extent on below-ground bacteria, fungi and other microbes that collectively function as a soil microbiome (*1*, *2*). Soil microbiomes consist of functionally diverse members providing beneficial services to plants, including nutrient acquisition, growth promotion, stress tolerance, and suppression of plant pathogens, but they can also contain pathogenic members that reduce plant fitness (*3*, *4*). Plant responses, which are causally linked to a soil microbiome, are referred to as microbiome feedbacks (*5*). This term is akin to plant-soil feedbacks describing the ecology of soil properties (more broadly, but including the microbiome) that influence plant performance (*6*, *7*). Microbiome feedbacks are highly relevant in agricultural contexts, as soil microbiome composition has been linked to agronomic traits of crops such as maize and potato (*8*, *9*), to field productivity (*10*), and to over- and under-yielding areas in fields (*11*, *12*). While different soil microbiomes have often been seen as drivers of differential plant responses (*13*, *14*), little is known about the mechanisms by which plants perceive complex soil microbiomes and mediate microbiome feedbacks.

Plants have evolved a sophisticated immune system that regulates interactions with beneficial microbes while defending against pathogens (*15–17*). Plant immunity operates through two key pathways: pattern-triggered immunity (PTI) and effector-triggered immunity (ETI). PTI is initiated at the cell surface by pattern-recognition receptors that recognize microbe-associated molecular patterns and provides basal defence to deter non-adapted microbes. In contrast, ETI is activated within the cells by nucleotide-binding leucine-rich repeat receptors (NLRs), which detect pathogen effectors or their activities, leading to definite immune responses (*18–20*). NLRs are divided into Toll/interleukin-1 receptor (TIR-NLRs; TNLs) and coiled-coil NLRs (CNLs). *Arabidopsis thaliana* Columbia-0 (Col-0) (hereafter: Arabidopsis) encodes 54 TNLs and 88 CNLs, highlighting the complexity of the plant immune system (*21*). Both PTI and ETI rely on signalling molecules such as salicylic acid (SA) and reactive oxygen species (ROS) (*19*, *20*). Although these pathways were primarily studied in the context of binary interactions with pathogenic or beneficial microbes, recent evidence suggests that PTI and ETI, and signalling via SA and ROS also influence plant-associated microbiomes. These immune pathways shape microbiome composition, modulating microbial interactions and contributing to overall plant health and resilience (*16*, *22–24*).

To study microbiome feedbacks, we developed an experimental framework based on two distinct soil microbiomes in the same soil type. These soil microbiomes are generated by growing wild-type maize, which produces benzoxazinoids (BXs), or BX-deficient mutant maize. BXs are bioactive compounds of *Poaceae* (*25*) that, among multiple functions, shape the root and rhizosphere microbiomes of plants (*14*, *26*, *27*). After three months of growth, the wild-type and mutant plants are removed, leaving behind BX-conditioned (BX_{plus}) and its control (BX_{minus}) soil microbiomes,

respectively. We have described growth and defence feedbacks of maize and wheat in response to BX_{minus} and BX_{plus} soil microbiomes (*14*, *28*), and we have proven agronomic relevance of these microbiome feedbacks (*28*, *29*). Recently, we reported that such microbiome feedbacks also exist in the model plant Arabidopsis (*30*). The reference accession Col-0 responded with improved growth and enhanced defence when grown on the BX_{plus} compared to the BX_{minus} soil microbiome. As a plausible mechanistic explanation for this apparent lack of a growth-defence trade-off, the plants growing on the BX_{plus} soil microbiome were primed for SA defences (*31*). Through sterilization and microbiome complementation experiments, we demonstrated that the feedbacks were BX-dependent, but that the soil microbiomes drove the differential plant responses (*14*, *28*, *29*).

Microbiome feedbacks often differ between different genotypes of response plant (*32*, *33*). Also, in our work with maize and wheat responding to BX_{minus} and BX_{plus} soil microbiomes, we had observed a genetic component in microbiome feedbacks (*14*, *28*), but the underlying genetic basis for such feedbacks to soil microbiomes remains unknown. Here, we aimed to uncover the genetic basis underlying the microbiome feedbacks in Arabidopsis Col-0. To this end, we harnessed the genetic diversity among Arabidopsis accessions to study their growth feedbacks and used high-throughput phenotyping in combination with genome-wide association (GWA) mapping (**Extended Data Fig. 1**). We identified and functionally validated a yet uncharacterized TNL driving differential plant growth on the two soil microbiomes in the reference accession.

Results

Arabidopsis displays substantial phenotypic variation in microbiome feedbacks

Col-0 responded to the BX_{plus} soil microbiome with larger rosettes compared to the BX_{minus} soil microbiome, confirming earlier work (**Fig. 1a**, (*30*)). The effect size of the growth feedback was less pronounced at earlier timepoints, and a linear-mixed-effects model revealed a positive *time* × *microbiome* interaction, indicating that BX_{plus} plants grow faster than BX_{minus} plants over time (**Fig. 1b**). We set out to identify candidate loci that confer this growth feedback in this accession.

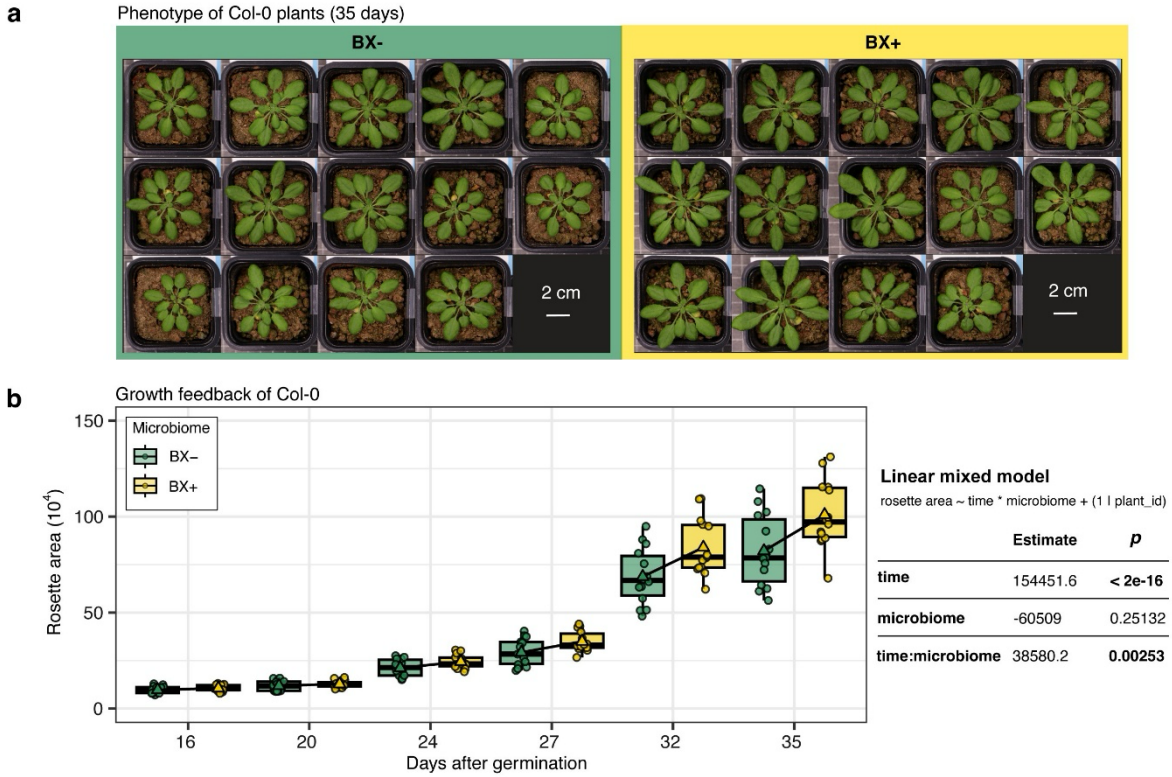

Figure 1. Growth feedbacks of Col-0 plants in response to the two soil microbiomes. (**a**) Phenotypes of Arabidopsis Col-0 plants grown on the BX_{minus} and BX_{plus} soil microbiomes at 35 days after germination. (**b**) Time course growth feedbacks of Arabidopsis Col-0 plants grown on the BX_{plus} compared to the BX_{minus} microbiome (points = individual plants). Linear-mixed-effects model of Col-0 rosette area across *time* and *microbiome* (minus vs plus).

We grew 410 natural, genome-sequenced Arabidopsis accessions (*34*) in both control (BX_{minus}) and BX-conditioned (BX_{plus}) soil microbiomes in a climate chamber equipped with an automated top-view imaging system. The process from imaging to determination of rosette area and feedback calculation is illustrated with the two contrasting accessions IP-Hue-3 and Hadd-3, which grew better and worse on the BX_{plus} soil microbiome, respectively (**Fig. 2a**). Plants were imaged twice a day, and plant morphometric traits were extracted using ARADEEPOPSIS (*35*). We focussed on the first 20 days after germination (DAG) to avoid confounding phenotyping effects such as early flowering and overlapping leaves. We used rosette area as a measurement of plant size to calculate the daily growth

143 feedback as the difference in rosette area between BX_{plus} and BX_{minus} microbiomes, i.e., the accessions
144 IP-Hue-3 and Hadd-3 exhibited positive and negative feedbacks, respectively (**Fig. 2b**).
145 Screening of natural accessions revealed substantial variation in growth feedbacks to BX_{plus} and
146 BX_{minus} microbiomes (**Fig. 2c**, **Dataset 1** and **Suppl. File 1**). Consistent with the above, Col-0 expressed
147 a subtle positive feedback at the early timepoint of the GWA experiment. Across the 410 accessions,
148 48% (196 accessions) displayed positive feedbacks, while 52% (214 accessions) showed negative
149 feedbacks. At the two extremes of the distribution, the two soil microbiomes accounted for ~2-fold (IP-
150 Hue-3) and >3-fold (Hadd-3) differences in rosette area in response to the two microbiomes. The
151 observed feedback responses were independent of the accessions' geographical origin (**Fig. 2d**,
152 **Extended Data Fig. 2a**).
153 Since BXs are allelopathic to plants (*36*, *37*), we tested whether the accessions' growth
154 differences could be due to varying sensitivity to residual BXs in soil. BXs differ between the two soil
155 variants, with MBOA as the most abundant BX compound (*29*, *38*). We screened a subset of accessions
156 with the strongest opposing growth feedbacks for sensitivity to MBOA. All accessions exhibited shorter
157 roots in the presence of MBOA (**Extended Data Fig. 3a**, **Dataset 2** and **Suppl. File 2**), which is
158 indicative of phytotoxicity. However, there was no correlation between the microbiome response of the
159 accessions and their sensitivity to MBOA (**Extended Data Fig. 3b**). These results indicated that the
160 observed growth feedbacks are not linked to varying sensitivity to the BXs present in the soil.
161 In conclusion, we found substantial phenotypic variation in growth feedbacks of Arabidopsis
162 accessions to two soil microbiomes, providing a powerful resource for association studies on the
163 genetics that drive the differences in feedbacks.

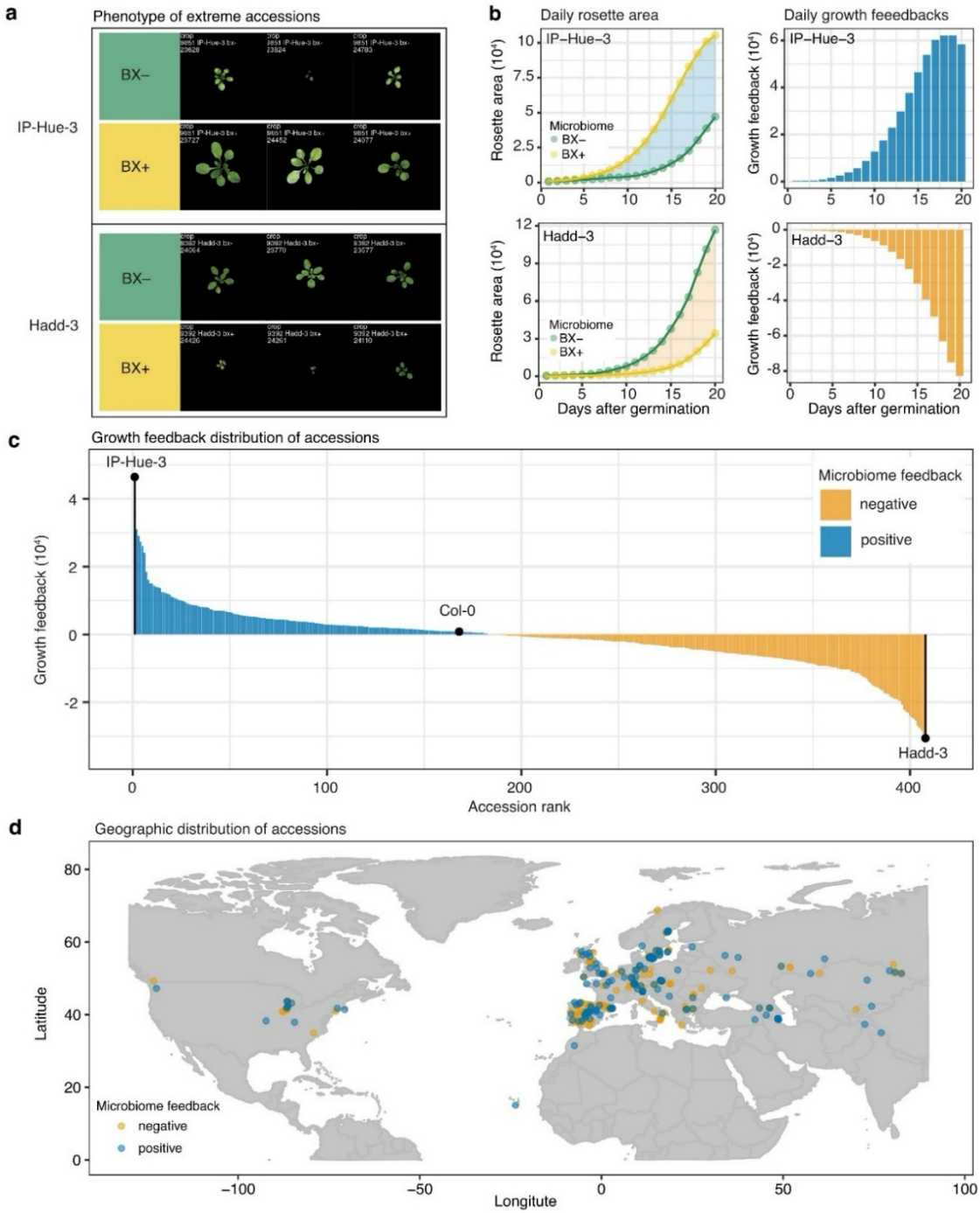

Figure 2. **Natural variation in growth feedbacks among Arabidopsis accessions**. (**a**) Growth of the two Arabidopsis accessions (IP-Hue-3 and Hadd-3) that exhibited the largest opposing growth feedbacks in response to the BX_{minus} and BX_{plus} microbiome at the conclusion of the experiment (20 days after germination (DAG)). (**b**) The daily rosette area measured in pixels extracted by ARADEEPOPSIS (left), growth feedback ($BX_{plus} - BX_{minus}$) (right) for the first 20 DAGs for IP-Hue-3 and Hadd-3 grown on the two soil microbiomes. Shaded areas (left) and coloured bars (right) indicate positive (blue, IP-Hue-3) or negative (orange, Hadd-3) microbiome feedbacks in response to the BX_{plus} microbiome. (**c**) Microbiome feedback of the 410 *A. thaliana* accessions used in the genome-wide association study at the conclusion (DAG 20) of the experiment. The position of IP-Hue-3, Hadd-3 and Col-0 are indicated on the graph. Data is from two phenotyping experiments (experiment I and II, **Table S1**), each consisting of a subset of 210 accessions (3 replicates per accessions per soil), with 10 overlapping accessions present in each of the experiments. (**d**) The map shows the geographic distribution of these accessions, coloured by their microbiome feedback (blue for positive; orange for negative).

177 ***Candidate gene loci are involved in plant growth and defence***

178 We performed a genome-wide association study (GWAS) using the phenotypic variation in growth
179 feedbacks of the 410 accessions (**Fig. 2c**) and employed a linear mixed model, accounting for population
180 structure (*39*). Noting temporal variation in daily growth feedbacks (**Extended Data Fig. 2b**), we ran
181 separate GWAS on daily data and calculated associations between single nucleotide polymorphisms
182 (SNPs) and the phenotypes for each of the 20 DAGs (**Dataset 3**).

183 Across daily GWAS runs, we identified three genomic regions with significant associations to
184 the growth feedback (**Fig. 3a**, **Dataset 3** and **Suppl. File 3**). Genes in the regions of the three peaks
185 were related to plant growth and plant defence. We then focused on SNPs that were significant for
186 multiple consecutive days in the repeated GWAS (see Methods). The top-ranked SNP (chromosome 3,
187 position 16203882) was in peak #2 (**Fig. 3a**), of which an alternative allele was found in 11 accessions
188 (**Fig. 3b**, **c**). On average, these accessions showed better growth in response to the BX_{plus} microbiome
189 compared to accessions with the reference allele. The SNP is in close proximity to the TNL receptor
190 gene *AT3G44630* (position 16200156; 3.7kb upstream) and a more distal second TNL (*AT3G44670*;
191 position 16218427; 14.5kb downstream; **Fig. 3d**). We focussed on the uncharacterized *AT3G44630*
192 because of i) the closer physical proximity to the top-ranking SNP (**Fig. 3d**), and ii) the differential
193 expression of *AT3G44630* in roots of Arabidopsis grown on BX_{minus} and BX_{plus} soils (*30*). In fact, from
194 the 33 candidate genes identified from the top 100 GWA peaks, only *AT3G44630* was both in close
195 proximity to a significant GWA peak (**Fig. 3a**) and displayed BX-dependent differential expression in
196 the roots of Col-0 (**Fig. 3e**). We named this gene *Mediator of Microbiome Feedback 1* (*MMF1*).
197 Structural predictions indicated high similarity to the well-characterized TNL, Recognition of
198 Peronospora Parasitica 1 (RPP1, (*40*)), suggesting that MMF1 also functions as a tetrameric TNL
199 resistosome (**Fig. S1**, **Suppl. Results**). However, unlike RPP1, MMF1 contains unique N- and C-
200 terminal extensions. Taken together, GWAS identified a genomic locus on chromosome 3 that includes
201 *MMF1* as a candidate gene that could explain the differential growth feedbacks of Arabidopsis
202 accessions in response to the BX microbiomes.

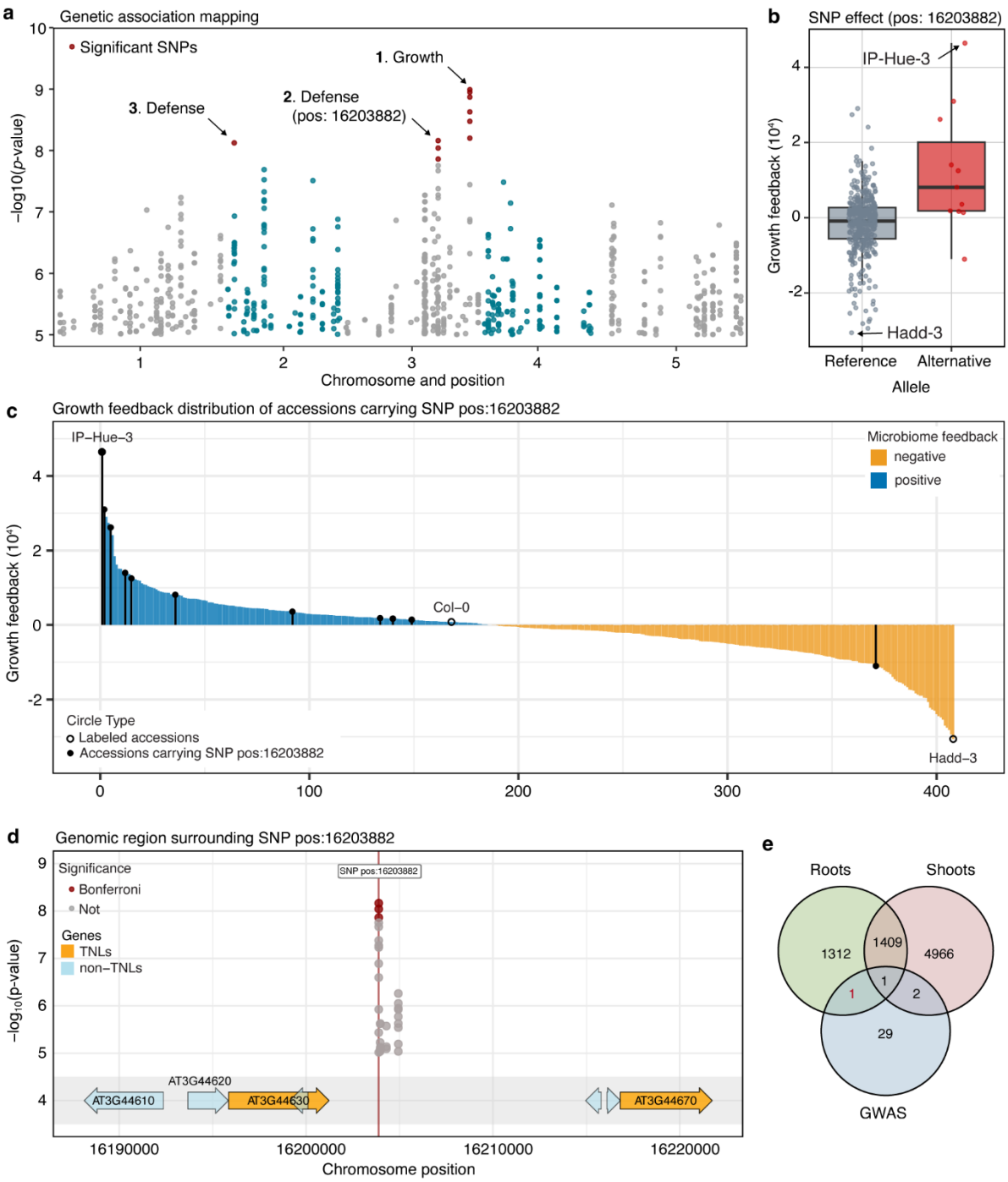

Figure 3. **Genetic association mapping of growth feedbacks in response to the BX_{plus} microbiome**. (**a**) Manhattan plot showing the -$\log_{10}$-transformed *p*-values for the top 500 single nucleotide polymorphisms (SNPs) across the 5 chromosomes of Arabidopsis. SNPs that are significantly associated with growth feedbacks after Bonferroni correction are shown in red. The biological functions of genes adjacent to the three top-ranking SNPs are indicated. (**b**) Average growth feedback among accessions carrying the alternative allele of the SNP at position 16,203,882 (positive feedback) compared to those with the reference allele (no or negative feedback). (**c**) Feedback distribution curve with accessions carrying the alternative allele of the SNP at position 16,203,882 indicated with black lines and filled circles. (**d**) The genomic region (50 kb) flanking the SNP at position 16,203,882, including the two TNL genes *AT3G44630* (*MMF1*) and *AT3G44670*. (**e**) Venn diagram showing the intersection between the genes located closest to the top-ranking 100 SNPs in (**a**), and genes differentially expressed (false discovery rate < 0.05; empirical Bayes' shrinkage, DESeq2) in the root and shoot transcriptome of Col-0 grown on the BX_{plus} and BX_{minus} microbiome (data from ref (*30*)).

216 ***MMF1 mediates differential microbiome feedbacks***

217 To validate the function of *MMF1* in microbiome growth feedbacks, we focussed on the reference
218 accession Col-0 in which the positive feedback was first observed (**Fig. 1**). We phenotyped two mutant
219 T-DNA insertion lines in Col-0 background for their response to the BX_{minus} and BX_{plus} microbiomes.
220 At the transcriptional level, the *mmf1-1* and *mmf1-2* lines are knockdown and knockout mutants,
221 respectively (**Extended Data Fig. 4**). Feedback assays were terminated at 35 DAG, when differential
222 growth feedbacks were consistently visible in previous experiments with Col-0 (**Fig. 1**). Both mutants
223 resembled the wild type in overall appearance - aside from slightly reduced size - and displayed no
224 disease symptoms (**Fig. 4a**, **Dataset 4** and **Suppl. File 4**). Consistent with the initial experiments (**Fig.
225 1**, (*30*)) and the GWAS experiment (**Fig. 2c**), wild-type plants expressed positive growth feedbacks in
226 response to the BX_{plus} microbiome, with higher fresh weight and larger rosette area compared to those
227 growing on the BX_{minus} microbiome (**Fig. 4b**). In contrast, both *mmf1* mutants lost the positive growth
228 feedback to the BX_{plus} microbiome, reflected in fresh weight and rosette area. This phenotype was
229 reproducible in two additional experiments using independently conditioned soil batches (**Extended
230 Data Fig. 5a**, **b**) and supported by a linear mixed-effects model (LMM) and estimated marginal means
231 (EMM) across all three experiments (**Extended Data Fig. 5c**). The line-specific estimates confirmed
232 that wild-type plants significantly responded to the BX_{plus} microbiome with enhanced fresh weight
233 (LMM: $p < 0.001$; EMM: $\beta = 0.036$, $p < 0.001$) and rosette area (LMM: $p = 0.023$; EMM: $\beta = 1.6 \times$
234 10^5, $p = 0.024$), while the effect of the BX_{plus} response was attenuated in *mmf1-1* (fresh weight: LMM:
235 $p = 0.055$; EMM: $\beta = 0.006$, $p = 0.583$; rosette area: LMM: $p = 0.25$; EMM: 4.1×10^4, $p = 0.587$) and
236 lost in *mmf1-2* (fresh weight: LMM: $p = 0.033$; EMM: 0.004, $p = 0.698$; rosette area: LMM: $p = 0.089$;
237 EMM: 9.6×10^3, $p = 0.891$). Complementary to the mutant analysis, we performed genetic
238 complementation of the *mmf1-2* mutant using a functional *MMF1* allele driven by the nopaline synthase
239 promoter. In these lines, the growth feedback was partially restored (**Fig. S2**, **Suppl. Results**),
240 confirming that the loss of *MMF1* is responsible for the absence of the differential growth feedback in
241 *mmf1* mutants. The genetic validation with mutant and complementation lines allowed to conclude that
242 a functional MMF1 is required for the differential growth feedback of Col-0 in response to the two soil
243 microbiomes.

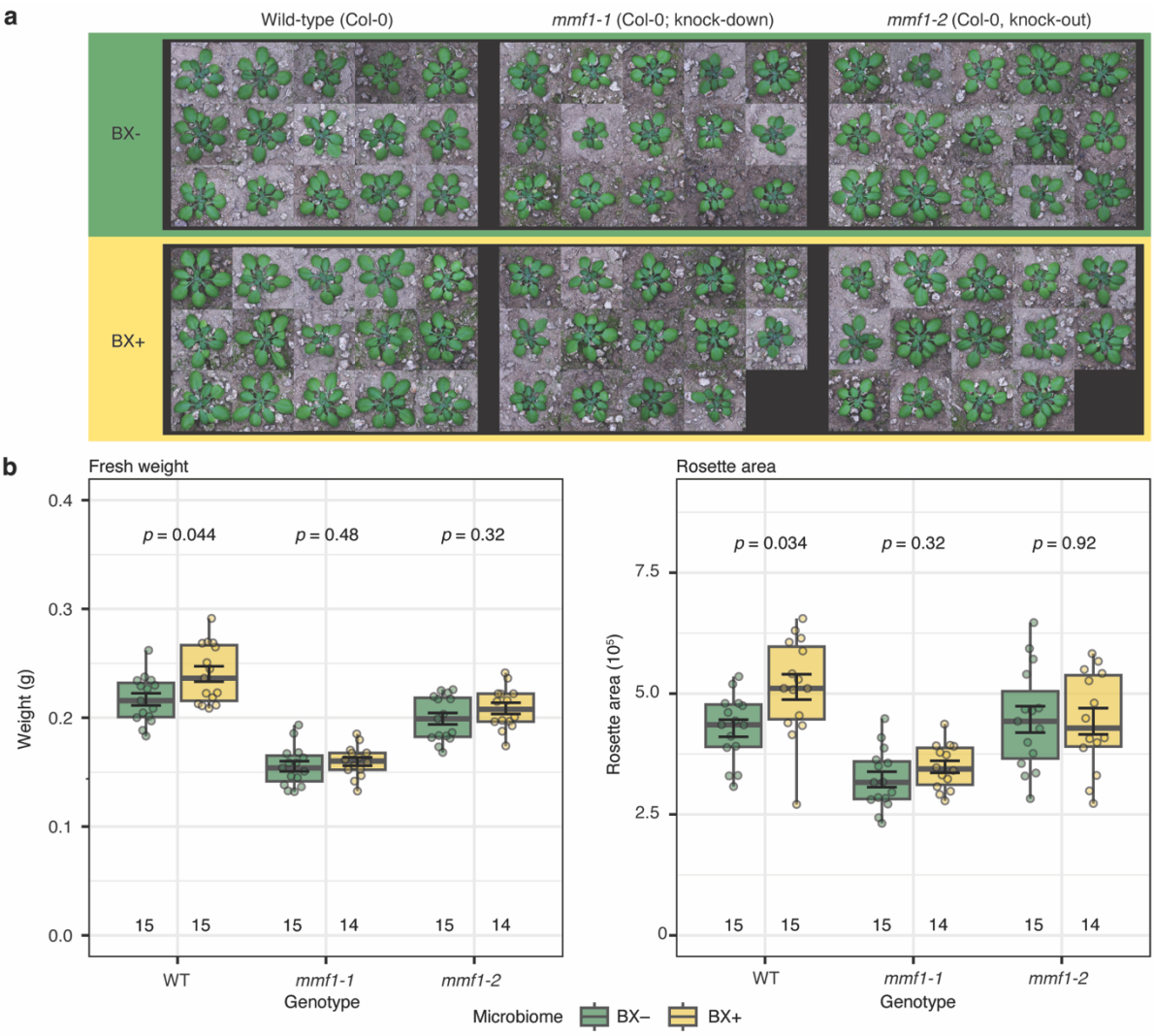

Figure 4. **MMF1 is involved in growth feedback responses to the BX_{plus} microbiome**. (**a**) Representative rosettes of 6-week-old Col-0 (WT) and two independent *mmf1* T-DNA insertion mutants (*AT3G44630*) grown on BX_{minus} and BX_{plus} soil microbiomes (experiment IV, **Table S1**). Scale bar, 2 cm. (**b**) Fresh weight (left) and rosette area (right; in pixels) after 6 weeks of growth for the genotypes in (**a**). The findings were reproduced in two additional experiments (experiments III and V) on two separately conditioned soil batches. Differences were analysed with a two-way ANOVA (*line* × *microbiome*) followed by Benjamini–Hochberg FDR correction; adjusted *p*-values are reported. Sample sizes (n) are given below each boxplot. Points represent individual plants.

The plant immune system relies on two TNL signalling pathways: Enhanced Disease Susceptibility 1 (EDS1) together with Phytoalexin Deficient 4 (PAD4) lead to resistance, and EDS1 jointly with Senescence-Associated Gene 101 (SAG101) induce hypersensitive responses and cell death (*41*). To test the involvement of the two TNL signalling pathways in microbiome feedbacks, we performed feedback assays with *eds1*, *pad4* and *sag101* mutant plants (*42*, *43*). These mutants showed no altered growth phenotypes or obvious disease symptoms in response to BX_{minus} or BX_{plus} soil microbiomes (**Extended Data Fig. 6a**). Similar to wild type, the three immune signalling mutants expressed positive growth feedbacks in response to the BX_{plus} soil microbiome (**Extended Data Fig. 6b**). Hence, single-gene knockouts in EDS1, PAD4 and SAG101 do not disrupt immune signalling that

leads to growth feedbacks, or alternatively, suggest that this process may be independent of these two classical pathways.

MMF1 affects root bacterial community assembly sourced from the BX_{plus} soil microbiome

In earlier work, we found differential microbiomes on roots of plants with differential growth feedbacks (*14*, *30*). Because *MMF1* encodes a defence-related protein, we profiled the root bacterial, fungal and oomycete communities recruited by wild-type and *mmf1* mutant plants when grown in BX_{minus} and BX_{plus} soils. The detailed microbiome analysis is documented in **Dataset 5** and **Suppl. File 5**. We utilised hamPCR (*44*), which determines microbial load relative to host tissue, for microbiome analysis and noticed in factorial ANOVA of microbial loads that the interaction term between the *line* (WT and *mmf1-2*) and *microbiome* (BX_{minus} and BX_{plus}) factors was close to significance for bacteria, but not for fungi or oomycetes (**Extended Data Fig. 7a**). Bacterial load was significantly higher in the roots of wild-type plants compared to *mmf1* mutants on the BX_{plus} microbiome. While alpha diversity (measured with Shannon index) did not differ between the factors *line* (WT and *mmf1*-2) and *microbiome* (BX_{minus} and BX_{plus}; **Extended Data Fig. 7b**), they impacted the compositions of the root microbial communities (beta diversity tested with Permutational Multivariate Analysis of Variance (PERMANOVA)). Source *microbiome* accounted for little variation in bacterial (R^2 = 4.6%, p = 0.059), fungal (R^2 = 3.0%, p = 0.25) and oomycete communities (R^2 = 4.7%, $p < 0.05$; **Fig. 5a**). For *line* however, we found significant differences in bacterial – but not fungal or oomycete – communities between wild type and *mmf1* mutants (R^2 = 5.9%, $p < 0.05$) and also in their interaction of the factors *line* with *microbiome* (R^2 = 4.5%, $p < 0.05$). The interaction effect indicated that the root microbiome of the mutant differed from wild type in only one soil type. Pairwise PERMANOVA confirmed this with more and significant variation between wild type and mutants in the BX_{plus} (R^2 = 18.3%, $p < 0.01$) compared to the BX_{minus} (R^2 = 5.1%, p = 0.548) soil microbiome. In contrast, fungal and oomycete communities showed no differences between *line* and *microbiome* (**Extended Data Fig. 7b**). Constrained Analysis of Principal Coordinates (CAP) confirmed these findings: root bacterial communities clearly separated between wild type and mutant on the BX_{plus} but not the BX_{minus} soil microbiome (**Fig. 5b**), while fungal and oomycete communities showed minimal, non-significant separation (**Extended Data Fig. 7c**). Taken together, the *mmf1* mutant assembled a distinct bacterial root microbiome relative to wild-type plants, but only on the BX_{plus} source microbiome.

a

Bacteria

	R^2	P
Line	**5.9**	**0.025**
BX_{minus}	5.1	0.548
BX_{plus}	**18.3**	**0.001**
Microbiome	4.6	0.059
Line:microbiome	**5.4**	**0.017**

Fungi

	R^2	P
Line	3.1	0.23
Microbiome	3.0	0.25
Line:microbiome	2.3	0.89

Oomycetes

	R^2	P
Line	2.7	0.34
Microbiome	4.7	**0.019**
Line:microbiome	2.9	0.27

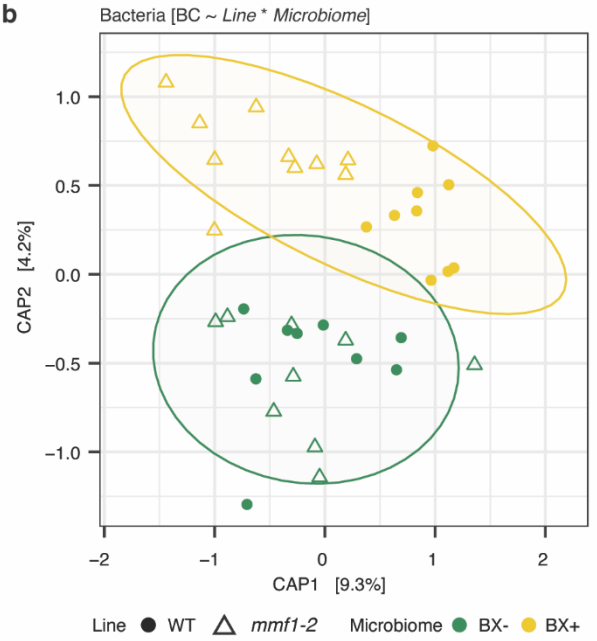

291 **Figure 5**. **Root microbiome profiling of wild-type and *mmf1-2* mutants grown on BX_{plus} or BX_{minus} soil**. (**a**)
292 The output of PERMANOVA on Bray-Curtis dissimilarities of bacterial, fungal and oomycete root microbiome
293 of Arabidopsis wild-type (WT; Col-0) and *mmf1-2* mutants grown on the BX_{minus} or BX_{plus} soils (sampled from
294 experiment IV, **Table S1**). The R^2 and p-values indicate the *line* and *microbiome* (conditioning) effects and their
295 interaction. Pairwise PERMANOVA for bacterial communities compares WT and *mmf1-2* mutants on each soil
296 condition; significant effects ($p < 0.05$) are indicated in bold. (**b**) Constrained Analysis of Principal Coordinates
297 (CAP) of Bray-Curtis dissimilarities [BC] for WT (filled circles) and *mmf1-2* mutant samples (open triangles)
298 grown on the BX_{minus} (green) or BX_{plus} (yellow) soils confirming the effects of the soil conditioning and lines
299 observed in the PERMANOVA analysis. Ellipses represent 95% confidence intervals for plants grown on BX_{minus}
300 (green) or BX_{plus} (yellow) soils. Axes show the percentage of variance explained by the first two principal
301 coordinates.
302

303 To identify the taxa that differed in abundance between roots of wild type and *mmf1* mutants
304 across the two soil microbiomes, we used DESeq2 (*45*) for modelling the same factors *line*, *microbiome*,
305 and their interaction. We retained only amplicon sequence variants (ASVs) with a false discovery rate
306 (FDR) < 0.05 for any model term. A total of 26 ASVs were differentially abundant: 18 by *microbiome*,
307 12 by *line*, and 20 by their interaction (**Extended Data Fig. 8**). ASVs assigned to *Pelomonas*, *Massilia*,
308 and *Asticcacaulis* were more abundant taxa in roots from plants grown in BX_{plus} soils. *Lechevalieria*,
309 *Variovorax*, and *Duganella* differed between genotypes and showed significant interaction effects.
310 *Pseudomonas*, *Lechevaleria* and *Aminobacter* were the most dominant ASVs, differing only by the
311 interaction term. We noticed that the latter all showed reduced abundance levels in the roots of *mmf1*
312 mutants grown on the BX_{plus} microbiome compared to wild type.

313 ***MMF1 is required for a defence-related transcriptional response***

314 To obtain first insights into how MMF1 contributes to positive growth feedbacks, we analysed the root
315 transcriptomes of wild-type and *mmf1-2* mutants in response to both soil microbiomes (detailed
316 transcriptome analysis documented in **Dataset 6** and **Suppl. File 6**). Analogous to the microbiome
317 analysis, we first examined the contributions of the factors *microbiome* and *line* on the transcriptome
318 using PERMANOVA. *Microbiome* accounted for 29.0% (based on R^2, $p < 0.01$), *line* for 33.7% ($p <$
319 0.01), and their interaction for 12.4% ($p < 0.01$) of the transcriptomic variation (**Fig. 6a**). Again, the
320 significant interaction term revealed that mutant and wild type responded differently to the two soil
321 microbiomes. Pairwise PERMANOVA again revealed greater variation in wild type ($R^2 = 79.7\%$, $p <$
322 0.01) compared to mutant ($R^2 = 10.8\%$, $p = 0.349$) plants in response to the two microbiomes. Principal
323 Component (PC) analysis confirmed a clear separation of wild-type individuals between the two source
324 microbiomes (PC1, 48% of variation) and between plant lines (PC2, 16% of variance; **Fig. 6b**). Overall,
325 the strongest separation was between wild-type plants in response to the two microbiomes, whereas the
326 *mmf1* mutant transcriptomes clustered together.

327 Next, we analysed the transcriptomes at the gene level to determine the differentially expressed
328 genes (DEGs; $\log_2$ fold-change ≥ 1; empirical Bayes shrinkage, p values adjusted for FDR < 0.05).
329 Aligned with the microbiome analysis (**Fig. 5**), we found more DEGs between the lines in response to
330 the BX_{plus} (347 total; 230 up and 117 down in wild type) compared to the BX_{minus} soil microbiome (128
331 total, 68 up and 60 down; **Extended Data Fig. 9a, b**). Wild-type plants showed 563 DEGs in response
332 to the two microbiomes (107 down and 456 up; **Fig. 6c**). Surprisingly, not a single *microbiome*-specific
333 DEG was found in mutant plants (**Fig. 6d**). Taken together, a functional MMF1 leads to a strong
334 transcriptional reprogramming, mostly in response to the BX_{plus} soil microbiome.

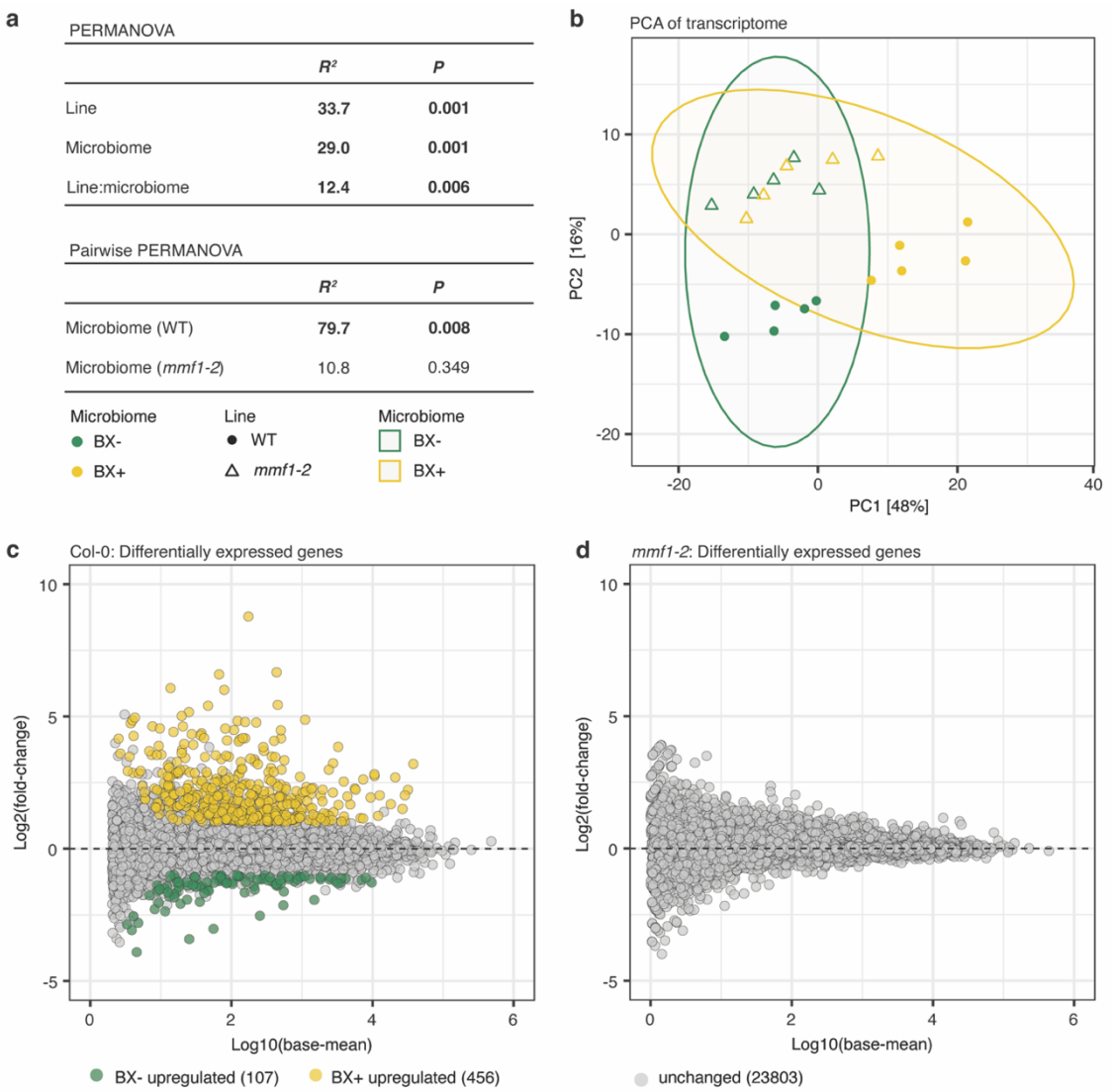

Figure 6. **Plants lacking MMF1 fail to mount a transcriptional response to a BX microbiome**. (**a**) The output of PERMANOVA on Euclidean distances of the root transcriptome of wild-type (WT) and *mmf1-2* mutant plants in response to the BX_{minus} and BX_{plus} microbiomes (sampled from experiment IV, **Table S1**). The R^2 and *p*-values summarize the effects of *line* (plant genotype) and *microbiome* (soil condition) along with their interaction. Pairwise PERMANOVA results compare the transcriptomes of WT and *mmf1-2* mutant plants when grown on the BX_{minus} soil microbiome compared to the BX_{plus} soil microbiome; significant effects are indicated in bold. (**b**) Principal component analysis (PCA) of the same root transcriptome confirms the *line* (WT, closed circles; *mmf1-2*, open triangles) and *microbiome* (BX_{minus}, green; BX_{plus}, yellow) effect of the PERMANOVA results. The axes display the percentage of variance explained by each principal component. (**c**) MA plots illustrating differentially expressed genes (DEGs) in WT between BX_{minus} and BX_{plus} (left), and the absence of DEGs in *mmf1-2* (right). Genes upregulated on the BX_{plus} microbiome (yellow) or BX_{minus} microbiome (green) are colour coded. Genes with an absolute $\log_2$ fold-change ≥ 1 and false discovery rate < 0.05 (empirical Bayes' shrinkage; DESeq2) are considered significant.

Finally, we performed co-expression and gene ontology (GO)-term enrichment analysis (underlying genes documented in **Dataset 6**) to characterise the transcriptional changes of wild-type plants in response to the two microbiomes (**Fig. 6c**). Hierarchical clustering identified clusters of co-expressed genes: four up- and three downregulated (**Fig. 7**, **Extended Data Fig. 9c**). Upregulated

353 processes included hypoxia (clusters #2 and #3) and immune responses (clusters #2 to #5). Processes
354 linked to hypoxia included the GO terms response to hypoxia and cellular response to hypoxia (**Dataset**
355 **6**). Upregulated immune processes included GO terms such as response to ethylene and systemic
356 acquired resistance (cluster #2), defence response to insects, and response to bacterial molecules (cluster
357 #3), indole metabolism and response to salicylic acid (SA; cluster #4), and hypersensitive response,
358 programmed cell death, and interaction with symbionts (cluster #5; see **Dataset 6** for the genes in each
359 cluster). Of note, several of these genes are typically involved in TNL-triggered immunity (*41*, *46*).
360 Downregulated processes included fatty acid biosynthesis, secondary metabolite biosynthesis and
361 malate transport (clusters #6 to #8; **Dataset 6**). In conclusion, wild-type plants, which achieved better
362 growth in response to the BX_{plus} soil microbiome, exhibited a strong transcriptional
363 reprogramming, most noticeably an upregulation of defence-related genes.

Figure 7. Gene ontology term enrichment reveals plant immune responses in response to the BX_{plus} microbiome. Hierarchical clustering and gene ontology (GO) term enrichment analysis performed on differentially expressed genes in wild-type roots grown on the BX_{plus} relative to BX_{minus} soil microbiomes. The top five most significantly enriched GO terms (Benjamini–Hochberg, $p < 0.01$) for each cluster are shown. Point size indicates the ratio of genes in a cluster mapping to the respective GO term, and point colour reflects the adjusted *p*-value (FDR corrected using Benjamini-Hochberg). Shading indicates clusters upregulated in plants grown on the BX_{plus} microbiome (yellow) or upregulated in plants grown on BX_{minus} microbiome (green). No significantly enriched GO terms were found for clusters 1 and 9. Bios., biosynthesis; metabol., metabolism; boil., biological; reg., regulation.

373 **Discussion**

374 While genotype-dependent microbiome feedbacks have been observed in many plant systems (*14*, *28*,
375 *29*, *33*), the mechanisms underlying plant responses to complex microbiomes remain largely
376 unresolved. Using our model system with Arabidopsis, where the reference accession Col-0 expresses
377 differential growth responses on two different soil microbiomes (*30*), we set out to uncover the genetic
378 basis of these microbiome feedbacks. Here, we used natural variation in growth feedbacks to BX_{plus} and
379 BX_{minus} soil microbiomes among natural Arabidopsis accessions (**Fig. 2c**) as a tool to uncover candidate
380 loci through which plants respond to different microbiomes in natural soils. We focussed on the gene
381 *AT3G44630*, which was in the proximity of the top-ranking SNP in the GWAS (**Fig. 3**), named this
382 TNL-receptor-encoding gene *MMF1*, and characterised it in the reference accession Col-0. Structural
383 modelling revealed that the predicted MMF1 tetramer shares high similarity with the tetrameric
384 resistosome structure of the well-characterized TNL RPP1 (*40*), including conserved TNL domains and
385 tetrameric assembly (**Fig. S1**). These predictions suggested that MMF1 may function as a TNL
386 perceiving microbial signals. In Col-0, *mmf1* mutants lacked three hallmarks of wild-type plants in
387 response to the BX_{plus} soil microbiome: they lost the positive growth feedback (**Fig. 4**), had an altered
388 root bacterial community and bacterial load (**Fig. 5**), and failed to trigger the defence-related
389 transcriptional response (**Fig. 6**). Given the molecular function of TNLs – to recognise microbially-
390 derived signals intracellularly and trigger an immune response (*20*) – our results support the following
391 mechanistic model (**Fig. 8**): When grown on the BX_{plus} soil microbiome, wild-type plants show
392 enhanced shoot growth resulting from a defence-related transcriptional response (**Fig. 7**). This MMF1-
393 dependent transcriptional response, together with the typical intracellular localisation of TNLs, suggest
394 that a bacterial (see below) signal of the BX_{plus} microbiome is perceived inside the root cells. This model
395 is consistent with the reduced shoot growth of wild-type plants on the BX_{minus} microbiome (in the
396 absence of the signal) as well as *mmf1* mutants on the BX_{plus} microbiome (lack of the receptor), and is
397 further supported by the lack of a defence-related transcriptome in *mmf1* mutants.

398 The plant responses, including a defence-related transcriptome and enhanced shoot growth,
399 coincided with an altered root microbiome (**Fig. 5**). While, overall, root microbiomes were similar
400 between soil sources, the bacterial load and communities of wild-type and *mmf1* mutant plants differed
401 significantly on the BX_{plus} but not on the BX_{minus} microbiome (**Fig. 5**). These data do not allow to
402 establish a causal link between the altered root microbiome and the differential shoot growth of the
403 genotypes. However, the observation suggests that a *bacterial* signal in the BX_{plus} microbiome, which
404 presumably triggers the defence-related transcriptome via the TNL MMF1, may be responsible.
405 Isolation of the bacterial species, possibly guided by the analysis of differentially abundant ASVs
406 (**Extended Data Fig. 8**) and the actual signal (i.e. a putative effector) are obvious future research
407 targets.

408 As part of the immune system, TNLs act as gatekeepers against opportunistic pathogens,
409 maintaining host health and microbiome homeostasis (*20*). Earlier work showed that Arabidopsis with
410 impaired ETI undergo microbiome dysbiosis in their leaves, and ultimately these plants have reduced
411 fitness (*24*, *47*). Analogously, in roots, we report microbiome dysbiosis in the mutant *mmf1* and
412 demonstrate that MMF1 is required for growth promotion in wild-type plants. Both examples imply
413 that TNLs integrate microbiome signals inside host cells for maintaining microbiome homeostasis and
414 host health. While TNLs and their signalling pathways have been predominantly studied in single-
415 pathogen and gene-for-gene interactions, this model faces a multiplicate challenge at the microbiome
416 level, with many more signals being present in a diverse microbiome (*16*). Thus, plant immune
417 responses rely on more complex signal integration when interacting with microbial communities
418 compared to single isolates (*16*, *47*). Moreover, there is evidence that signal integration may further
419 depend on TNL receptor dosage: recently, high TNL copy numbers within the *RPP-1*-like gene cluster
420 among Arabidopsis accessions were linked with reduced bacterial diversity in their phyllosphere (*48*).
421 Of note, the closest homolog of *MMF1* is *RPP1* (*49*), and additional TNL encoding genes are in the
422 proximity of the SNP most strongly associated with the variation in growth feedback among the tested
423 accessions (**Fig. 3d**). Here, we have shown that lack of MMF1 is sufficient for the loss of the previously
424 established growth feedback in Col-0, but future work is needed to test whether additional members of
425 the TNL family or their dosage (*48*) also contribute to feedback in other accessions.
426 We set out to identify a first genetic component through which plants respond to different
427 microbiomes in natural soils. The substantial variation in growth feedbacks among Arabidopsis
428 accessions (**Fig. 2c**) implies that there are additional components to discover. *MMF1* presents a first
429 genetic component for such feedbacks, but for now it only explains the enhanced growth and increased
430 defence of the reference accession Col-0 responding to the BX_{plus} microbiome. MMF1 activity alone
431 cannot explain the massive variation in growth feedbacks among the other accessions. For instance,
432 Hadd-3, which shares the reference allele of the top SNP with Col-0, grew more poorly on the BX_{plus}
433 microbiome, while IP-Hue-3 harboured the alternative SNP allele and grew much better than Col-0.
434 Solving this puzzle requires further analysis of the complex locus around the top SNP, and investigating
435 MMF1 variation of the extreme accessions such as Hadd-3 and IP-Hue-3. Together with the other
436 GWAS candidate loci (**Fig. 3a**), additional genetic components likely contribute to explaining the
437 massive variation in growth feedbacks among the accessions. It is also possible that the genetic
438 architecture of the identified locus shows a more complex, for example structural, variation pattern
439 across the study population.
440 In conclusion, the identified TNL receptor provides a relatively straightforward explanation for
441 the enhanced shoot growth of Col-0 on the BX_{plus} soil microbiome: MMF1 perceives a signal of the
442 BX_{plus} microbiome, triggers defences, and alters the root microbiome, which collectively coincide with
443 better shoot growth mediated by yet unknown mechanisms. This work contributes to understanding
444 host genetic pathways by which plants perceive complex soil microbiomes and mediate microbiome

445 feedbacks. Such knowledge may pave the way towards crops that leverage beneficial microbiome
446 feedbacks, ultimately improving yield in a more sustainable manner.
447

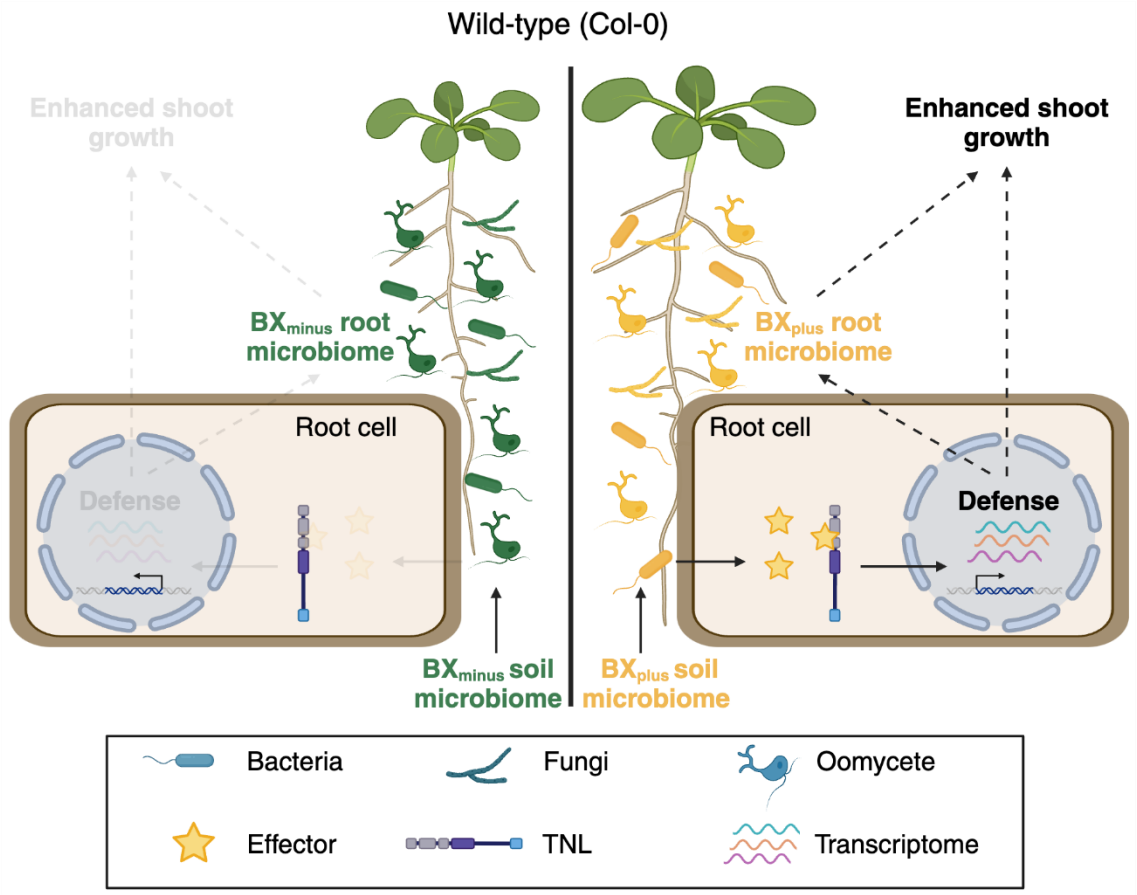

448 **Figure 8**. **Proposed model of microbiome feedbacks through MMF1 in Col-0 plants**. Plants with a functional
449 MMF1 receptor perceive a putative effector molecule that is present in the BX_{plus} soil microbiome, mounting a
450 defence response that coincides with an altered root microbiome and promoted plant growth. The absence of this
451 effector molecule in the BX_{minus} microbiome results in the lack of defence responses in plants grown on this soil
452 microbiome. Col-0 plants lacking the MMF1 receptor fail to perceive the effector molecule from the BX_{plus}
453 microbiome and do not mount defence responses; they have a different microbiome, and no enhanced shoot
454 growth is observed. Figure created with BioRender®.

455 **Methods**

456

457 ***Plant material***

458 The maize (*Zea mays* L.) genotypes B73 and *bx1* (B73) transposon insertion mutant (*50*) were used for
459 soil conditioning (see below). The 410 *Arabidopsis thaliana* (hereafter: Arabidopsis) accessions used
460 in the GWAS (see below) were obtained from the 1001 genomes project (The 1001 Genomes
461 Consortium, 2016). For a full list of the accessions used, see **Dataset 1**. Arabidopsis T-DNA insertion
462 mutants (AT3G44630) for *mmf1-1* (SALK_144159C) and *mmf1-2* (SALK_002318C) are in the Col-0
463 background and were obtained from the Nottingham Arabidopsis Stock Centre (NASC). Mutants were
464 confirmed for homozygosity and characterised by qPCR (**Extended Data Fig. 4;** primers in **Table S3**).
465 The mutant lines *eds1-12* (*42*), *pad4-1* (*51*), and *sag101-3* (*52*) in Col-0 background were kindly
466 provided by Prof. Jane Parker.

467

468 ***Generation of BX_{minus} and BX_{plus} soil microbiomes***

469 We used soil from an agricultural field site of Agroscope in Changins, Switzerland
470 (46°24'00.0"N6°14'22.8"E; three adjacent plots, Parcel 29, Parcel 30, or Parcel 31) and we generate the
471 distinct soil microbiomes either in the field or in the greenhouse using pots filled with that soil. Starting
472 from replicates of the same batch of unconditioned field soil, the two distinct microbiomes are generated
473 by growing of either wild-type maize (B73), which secrete benzoxazinoids (BXs) to the surrounding
474 soil, or BX-deficient mutant maize (*bx1* (B73)). After three months of growth, the plants and roots are
475 removed and the two maize lines "leave behind" BX-conditioned (BX_{plus}) and control (BX_{minus})
476 microbiomes in the soil. We then harvest either replicate soil cores (20 × 20 × 20 cm, conditioning in
477 the field) or soil from replicate pots (3 L, 13.1 cm deep and 20.2 cm diameter; conditioning in the
478 greenhouse), sieve the soil through a 1 cm^2 sieve and stored it at 4°C until the subsequent feedback
479 experiments. We described in detail the approach of generating BX_{minus} and BX_{plus} soil microbiomes
480 (we often referred to this as 'soil conditioning') including the physicochemical characteristics of the
481 soil (*14*, *28*, *38*), management practices and cropping history of the field site (*14*, *26*) and the conditions
482 for greenhouse conditioning (*14*, *28*, *30*). The batches of conditioned soils for this study, and the
483 experiments linked to soil batches are listed in **Table S1** and **S2**.

484

485 ***Microbiome feedback experiments***

486 We list the setups and purposes of different experiments (Exp. I to Exp. VII) with Arabidopsis grown
487 on BX_{minus} and BX_{plus} soil microbiomes in **Table S2**. For feedback experiments, the replicate soil
488 samples containing the BX_{plus} and BX_{minus} microbiomes were individually amended with sand, by
489 manually mixing in 20% (v/v) autoclaved quartz sand (*14*). Pots were equally filled by weight and
490 randomized across trays. Below we detail the specific setups and conditions for the high-throughput

491 phenotyping of the different Arabidopsis accessions (Exp. I and II) and the characterisation of wild-
492 type and mutant lines in Col-0 background (Exp. III - VII).
493 *High-throughput phenotyping of Arabidopsis accessions:* We performed two microbiome
494 feedback experiments; each experiment was done with 210 accessions (10 accessions repeated in both
495 runs) resulting in a total of 410 tested Arabidopsis genotypes (**Dataset 1**). In each experiment, every
496 accession was seeded on both BX_{minus} and BX_{plus} soils with 3 replicates (2 experiments of 210 accessions
497 x 2 soils x 3 replicates = 1260 pots). Plant cultivation and phenotyping was previously described and
498 the images of the first experiment were utilized to develop the phenotyping software ARADEEPOPSIS
499 (without comparing BX_{minus} and BX_{plus} soils) (*35*). In brief, plants were grown at the Gregor Mendel
500 Institute of Molecular Plant Biology, Vienna, Austria, in a custom-built growth chamber (YORK
501 Refrigeration), equipped with an environmental control unit (Johnson Controls) and a climate control
502 unit (Incotec) under long-day conditions (16h light [21°C], 8h dark [16°C], 140 $\mu E/m^2s$) with 60 %
503 relative humidity and watered twice per week by flooding. Plants were imaged twice daily, and plant
504 morphometric phenotypes extracted using the phenotyping software ARADEEPOPSIS (*35*). The
505 phenotypes were converted into "days after germination" phenotypes by taking the average of the two
506 measurements that happened on the same day. **Dataset 1** contains the source data and **Suppl. File 1**
507 documents the analysis.
508 *Feedback experiments with Arabidopsis mutants:* For microbiome feedback experiments
509 performed on Arabidopsis Col-0 mutant lines, we used greenhouse conditioned soils prepared as
510 described before. Seeds were stratified for 3 days in the dark at 4 °C and sowed on pots (5.5 × 5.5 × 5
511 cm) filled by weight. Plants were grown in a plant growth chamber (Percival, CLF Plant Climatics,
512 Wertingen, Germany) under short days with 10h light (100 $\mu mol\ m^{-2}\ s^{-1}$) (21 °C) and 14h darkness (18
513 °C) at 60% relative humidity. Plants were fertilized at day 14 and 21 after germination using 10 mL of
514 1:3 times diluted ½ strength Hoagland solution (*53*), watered 3 times per week by weight, and
515 randomized weekly. Analysis was blinded by adding barcodes to the pots for phenotyping which was
516 used to trace back sample names after analysis. Plants were photographed weekly and phenotyped using
517 the ARADEEPOPSIS pipeline to obtain the rosette area (plant region area) (*35*). Plants were grown for
518 6 weeks before the rosettes and roots were harvested for downstream analysis. **Dataset 4** contains the
519 source data and **Suppl. File 4** documents the analysis.
520
521 ***Genome-wide association study***
522 Genome-wide association studies (GWAS) search for associations between single nucleotide
523 polymorphisms (SNPs) in a genome and a phenotype (*54*). As phenotype we took the differential growth
524 feedback of the accessions on the two soil microbiomes, i.e. the mean growth on BX_{minus} was subtracted
525 from the mean growth on BX_{plus} soil microbiomes [$BX_{plus} - BX_{minus}$]. We focussed on the first 20 days
526 after germination (DAG) to avoid confounding effects of phenotypes like early flowering and
527 overlapping leaves. GWA was performed using an in-house Nextflow pipeline

528 (https://gitlab.lrz.de/beckerlab/gwas-nf) that wraps limix (*39*) and applies the same multi-trait model
529 used previously in (*35*). Only SNPs with a minor allele frequency of at least 1% were included. The
530 model estimates each SNP's "specific" effect on the trait "differential growth feedback". In this study,
531 we used plant_region_area as a trait (**Dataset 1**), and the specific effect reflects the difference in that
532 measurement between the soil conditions. The analysis was conducted independently for each day
533 because we noted temporal variation in daily growth feedbacks, and the resulting tables were combined
534 without re-adjusting the corrected p-values. SNPs were retained and visualized if they had a
535 $-\log_{10}$(adjusted p-value) of at least 5 on at least three consecutive days and a minor allele count of at
536 least 5. From these plots, we identified SNPs with a robust multi-day signal and analysed them further
537 using gwaR (https://github.com/Gregor-Mendel-Institute/gwaR). This allowed us to investigate the
538 genomic neighbourhood of those SNPs and pinpoint genes likely involved in the microbiome feedback
539 phenotype. The GWAS data are in **Dataset 3** and their analysis is documented in the **Suppl. File 3**. For
540 computational analyses, we used the BioHPC-Genomics compute cluster at the Leibniz Rechenzentrum
541 and the CLIP cluster at Vienna BioCenter (VBC).
542
543 ***GWAS candidate gene selection***
544 To identify candidate genes associated with BX-growth feedbacks, we performed the genome wide
545 association study (GWAS) with the 410 genome-sequenced accessions using their phenotypic diversity
546 in growth feedbacks (**Fig. 2c**). To account for population structure within the *Arabidopsis* accessions,
547 a linear mixed model was employed (*39*). We used the daily growth feedback data, which includes the
548 temporal dynamics (**Extended Data Fig. 2b**), and calculated associations between single nucleotide
549 polymorphisms (SNPs) and phenotypes for each of the 20 DAGs (**Dataset 3**). In essence, we performed
550 the GWAS using each day as a covariable in the analysis.
551 To impose stringency in SNP identification, we performed FDR correction and Bonferroni
552 correction of the *p*-values of SNPs that associated with the growth feedbacks (**Fig. 3a**, **Dataset 3**). Next,
553 we filtered the SNPs for those with a minor allele frequency of higher than 2.5 % to also include rare
554 SNPs associated with local and environmental adaptation (*55*), and those SNPs with significance
555 (Bonferroni correction) for at least three consecutive days. To isolate candidate genes, we used the
556 "get_nearest_genes" function from the gwaR package in R (https://github.com/Gregor-Mendel-
557 Institute/gwaR) to identify genes located near each candidate SNP. Finally, to select candidate genes
558 for functional validation, we screened the genes identified in the GWAS for overlap with differentially
559 expressed genes in the roots and shoots of Arabidopsis plants grown on a BX_{minus} and BX_{plus} microbiome
560 (*30*).
561
562 ***Validation of single T-DNA insertion in mmf1-2***
563 We validated that *mmf1-2* carries a single T-DNA insertion by long-read whole genome sequencing and
564 reference-guided assembly. High molecular weight DNA was extracted from leaves using the Machery-

565 Nagel NucleoBond HMW DNA kit according to manufacturer's instructions. Long-read sequencing
566 was carried out on an Oxford Nanopore Technologies promethion 24 instrument in a multiplexed run
567 on a R10.4 flow cell. After demultiplexing with dorado (https://github.com/nanoporetech/dorado)
568 adapters were trimmed using porechop, and the genome was assembled using flye (*56*), polished with
569 medaka (https://github.com/nanoporetech/medaka) and scaffolded against Col-CEN (*57*) using ragtag
570 (*58*) and annotations (araport11) from Col-CEN were lifted over using liftoff (*59*). The T-DNA insertion
571 in AT3G44630 was identified by aligning to the reference genome. The T-DNA sequence was used as
572 a query for BLAST against the *mmf1-2* assembly, returning only the insertion in AT3G44630
573 (**Extended Data Fig. 4d**).
574
575 ***Generation of MMF1 complementation lines***
576 To generate *MMF1* complementation lines in the *mmf1-2* mutant background, we used a binary vector
577 containing the full-length *Arabidopsis thaliana MMF1* gene (*AT3G44630*, transcript ID:
578 NM_180324.2) under the control of the nopaline synthase (NOS) promoter. The expression construct
579 was commercially synthesized and cloned by VectorBuilder (vector name: pPBV[Exp]-Hygro-
580 Nos>ath_AT3G44630[NM_180324.2]) and includes a hygromycin resistance cassette for plant
581 selection. The construct was introduced into *Agrobacterium tumefaciens* strain AGL-1 by
582 electroporation. Arabidopsis *mmf1-2* homozygous mutants were transformed using the floral
583 inoculation method (*60*). Transformed seeds were selected on Murashige and Skoog (MS) medium
584 supplemented with hygromycin (20–30 mg/L). Resistant T1 seedlings were transferred to soil, and
585 independent transgenic lines were screened for *MMF1* expression (**Fig. S2c**) and T3 lines used in
586 downstream phenotypic analyses.
587
588 ***MBOA allelopathic growth assays***
589 To test for the allelopathic effect of MBOA on plant growth, we grew different Arabidopsis accessions
590 on ½ MS (Duchefa, Haarlem, the Netherlands) plates containing 1.5% phytoagar (Duchefa, Haarlem,
591 the Netherlands) supplemented with 0.25 mM MBOA (Sigma Aldrich, St. Louis, USA) dissolved in
592 DMSO or on control plates supplemented with the same concentration (500 µL per L) of DMSO (*61*).
593 Seeds were stratified by incubating plates for 3 days at 4 °C. The plates were placed upright and grown
594 in a controlled growth chamber (Percival, CLF Plant Climatics, Wertingen, Germany) in short days
595 with 10 hours light (100 µmol m^{-2} s^{-1}) (21 °C) and 14 hours darkness (18 °C) at 60 % relative humidity.
596 After 10 days, the lateral root length was measured using the image software ImageJ (*62*).
597
598 ***Root microbiome profiling***
599 *DNA extraction:* For root microbiome analysis, 10 randomly selected *Arabidopsis* root systems were
600 removed from the pots, and excess soil carefully removed by hand. The root system was rinsed with
601 sterile ddH_2O to remove additional soil. The entire root system was flash frozen in liquid nitrogen and

602 stored at -80 °C until further processing. The roots were lyophilized for 24 h and grinded in 1.5 mL
603 Eppendorf tubes using a Retsch mill (Retsch GmBH, Haan; Germany) and 2 mm glass beads at 30 Hz
604 for 1 min. Approximately 20 mg of dry root material was used as the input for DNA extractions. DNA
605 extractions were performed in 96-well plates using the QIAGEN® MagAttract® PowerSoil® DNA KF
606 Kit (Qiagen, Germany) and the KingFisher™ Flex™ Purification System (ThermoFisher Scientific,
607 Waltham, MA) following the manufacturers guidelines. For all samples, the DNA concentration was
608 determined using the AccuClear® Ultra High Sensitivity dsDNA Quantitation Kit (Biotum, Fremont,
609 United States). For library preparation, DNA concentration was adjusted to 2 ng/µL with a Myra Liquid
610 Handler (Bio Molecular Systems, Upper Coomera; Australia), and 10 ng used for library preparation.
611 *Library preparation:* Library preparation for bacteria, fungi and oomycetes was performed
612 using an adapted two-step barcoded host-associated microbiome hamPCR protocol (*44*). Primers used
613 are documented in **Table S3**. For bacteria, the first PCR was performed using a combination of the
614 CS1-*fs*-799-F and CS2-*fs*-1193R frameshift (fs) (pooled in 5 equimolar concentrations) in
615 combination with the host specific *GIGANTEA* CS1-At-GI-F and CS2-At-GI-R primers in a single well.
616 We followed earlier work PCR settings for annealing temperature (*63*) and cycling conditions (*44*).
617 Briefly, the PCR settings were 94 °C for 2 min, and 10 cycles of 94 °C for 30 s, 55 °C for 50 s, 72 °C
618 for 30 s and finally 72 °C for 5 min. For fungi, the first PCR was performed with the internal transcribed
619 spacer (ITS) region primers ITS1fF and ITS2R with standard temperature (*64*) and cycle (*44*) settings.
620 The PCR settings were 94 °C for 3 min, and 10 cycles of 94 °C for 45 s, 50 °C for 60 s, 72 °C for 90 s,
621 and finally 72 °C for 10 min. For oomycetes, we adapted the ITS1-O_F1_G-46636 and 5.8s-O_R1_G-
622 46637 primers (*44*) with the CS1 and CS2 adapter sequences and utilised the same PCR settings as for
623 the fungi. PCR amplicons were purified using the ChargeSwitch® PCR Clean-Up Kit (Invitrogen,
624 Waltham, MA, USA) on a KingFisher™ Flex™ Purification System (ThermoFisher Scientific,
625 Waltham, MA, USA). The second PCR added unique barcodes to 5 µL of purified DNA using the
626 Fluidigm Access Array barcoding primers (Standard BioTools, California, USA). The cycling
627 conditions were 94 °C for 2 min, 25 cycles of 94 °C for 30 s, 60 °C for 30 s, 72°C for 60 s, and finally
628 extension 72°C for 10 min. Samples were again purified as before and quantified and pooled by adding
629 80 ng of each sample using a Myra Liquid Handler to create sub-libraries for bacteria, fungi and
630 oomycetes. The pooled bacterial sub-library was subsequently separated on an 1.5 % agarose gel, the
631 bacterial and GIGANTEA fragments excised, and gel purified using the Wizard® SV Gel and PCR
632 Clean-Up System (Promega, Madison, Wisconsin, USA). The final bacterial sub-library was created by
633 scaling the purified bacterial and GIGANTEA amplicons in a 24:1 ratio (bacteria:GIGANTEA) to
634 reduce the amount of plant reads during sequencing. Five random samples were duplicated during
635 library preparation and left unscaled to bioinformatically rescale the scaled samples (see ref (*44*) for
636 details). The final sequencing library was created by pooling the sub-libraries in a DNA ratio of 87.5%
637 (963 ng) scaled bacteria, 5.5 % (60 ng) unscaled bacterial samples and 3.5 % (39 ng) each for fungal

638 and oomycetes. The library was paired end sequenced on an Illumina MiSeq instrument (v3 chemistry,
639 300 bp paired end) at the NGS platform (https://www.ngs.unibe.ch) of the University of Bern.
640 *Bioinformatics*: MiSeq reads were quality checked with FastQC v0.11.8 (Babraham Institute,
641 Cambridge, United Kingdom). Barcodes were removed previously by the NGS platform and written to
642 the sequence headers. With this information the data was demultiplexed and primers were removed
643 using cutadapt v3.4 (*65*). Following the methods from (*29*), quality filtering, read merging and amplicon
644 sequence variant (ASV) inferring was performed with the dada2 package v1.26.0 (*66*) in R v4.2.0 (R
645 Core Team 2022). Taxonomic assignment were done using naïve Bayesian classifier with a DADA2
646 formatted version from the SILVA v. 132 database (*67*) for bacteria and the FASTA general release
647 from UNITE v8.3 for fungi. To improve taxonomy assignment, the taxonomy was assigned again with
648 the IDTAXA classifier using the SILVA r138 and UNITE 8.2 databases from DECIPHER v2.26.0 (*68*)
649 and replaced wherever IDTAXA assigned more taxonomic levels than the naïve Bayesian classifier.
650 Bacterial ASVs assigned as Eukarya, Archaea, Cyanobacteria or Mitochondria and fungal ASVs
651 belonging to Protista, Plantae, Protozoa or Animalia were discarded. Calculations were performed at
652 the sciCORE (http://scicore.unibas.ch/) scientific computing centre of the University of Basel.
653 *Statistical analysis:* Statistical analyses were performed with the vegan package v.2.6.4 (*69*) in
654 R v4.2.0. Following the strategies described before (*70*), we normalised the data for bacteria, fungi and
655 oomycetes by rarefication. Rarefaction thresholds per sample were defined as 65'000 for bacteria, 400
656 for fungi and 5'700 for oomycetes (*70*). Outlier detection was performed with CLOUD using Bray-
657 Curtis (BC) distances from the rarefied data for each condition and each treatment individually (*71*).
658 The nearest number of neighbours were set to 60% of the sample size and we chose an empirical outlier
659 percentile of 0.1. As described before (*44*), microbe-to-host ratios were reconstructed and the microbial
660 load of each sample was quantified. Using a count table scaled by the microbial load, we performed
661 ordinations based on Bray-Curtis dissimilarity matrices using R package phyloseq (*72*) and visualised
662 it in a Constrained analysis of principle coordinates (CAP). We performed Permutational Multivariate
663 Analysis of Variance (PERMANOVA) with 999 permutations with the adonis function from the vegan
664 package to quantify the effects of our experiment. To identify taxa differentially abundant across
665 genotypes, microbiomes, and their interaction, we used the DESeq2 (*45*) package (v1.38.3) in R. A full
666 factorial model was fitted with the formula ~ *line* * *microbiome*, where *line* denotes host genotype (WT
667 and *mmf1-2*) and *microbiome* referred to BX_{minus} and BX_{plus} soils. This design allowed for estimation of
668 main effects and interaction terms while accounting for variance structure and normalization of count
669 data using DESeq2's internal size factor estimation. ASVs were considered significantly differentially
670 abundant for a given model term if they had an adjusted *p*-value (Benjamini–Hochberg FDR) < 0.05.
671 ASVs significant for any of the three terms (*line*, *microbiome* and their interaction) were retained for
672 downstream visualization. To aid interpretability of the heatmap, group-wise average relative
673 abundances (collapsed by genotype × microbiome) were computed from normalized counts and square-
674 root transformed to reduce the influence of highly abundant ASVs. ASVs were first grouped based on

675 their significance in the DESeq2 model as follows: (1) *microbiome-only*, (2) *line-only*, (3) *interaction-*
676 *only*, and (4) *multi-category* (significant for multiple terms). Within each group, ASVs were sorted by
677 their average abundance across all samples. Genus-level taxonomy was appended to each ASV ID
678 where available. The microbiome data is in **Dataset 5** and its analysis is documented in **Suppl. File 5**.
679
680 ***Transcriptome analysis***
681 *RNA extraction, library preparation and sequencing:* Roots from 6-week-old Arabidopsis plants were
682 carefully removed from the soil. Excess soil was removed by briefly rinsing the roots in sterile ddH_2O
683 and dried using a paper towel. The roots were then flash frozen in liquid nitrogen and homogenized in
684 a 1.5 mL Eppendorf tube using a plastic micro pestle (Carl Roth, Karlsruhe, Germany). Total RNA was
685 extracted using the RNeasy Plant Mini Kit (Qiagen, Hilden, Germany) with on-column DNase
686 treatment with the RNase-Free DNase kit (Qiagen, Hilden, Germany) following the manufacturer's
687 protocol. RNA integrity was assessed using a Fragment Analyzer (Agilent Technology, Santa Clara,
688 California, USA). RNA concentration was determined fluorometrically using the Qubit RNA HS Assay
689 Kit (Thermo Fisher, Waltham, Massachusetts, USA). Libraries were prepared using the TruSeq
690 Stranded mRNA kit (Illumina, SanDiego, California, USA) with 200 ng total RNA as input. Library
691 preparation and sequencing was performed at the Genomics Facility
692 (https://bsse.ethz.ch/genomicsbasel) of the University of Basel. Sequencing (51 bp paired end) was
693 performed on an Illumina Novaseq® 6000 System (Illumina, SanDiego, California, USA) with an SP
694 slow cell.
695 *Bioinformatics and statistics:* Reads were aligned to the *Arabidopsis thaliana* TAIR10
696 reference genome and read counts determined using STAR 2.7.9a (*73*). The raw data processing was
697 performed at the scientific computing facility of the University of Basel (http://scicore.unibas.ch/).
698 Sample outliers were identified using a combination of generalized principal component analysis and
699 by analysing Poisson distances across samples. Sample clustering was performed using variance
700 stabilizing transformations on the normalized gene counts. Differential gene expression analysis was
701 performed in R using DESeq2 (*45*), a method for differential analysis of count data using a negative
702 binomial generalized linear model with shrinkage estimation of dispersions and fold changes. Co-
703 expression analysis was performed with the R package coseq v1.18.0 (*74*). Clustering of the co-
704 expressed genes was performed by running a Gaussian mixture model and arcsine transformation of
705 normalized expression profiles 20 times to identify the optimal number of clusters (*74*). The
706 transcriptomic data is in **Dataset 6** and the documented analysis in **Suppl. File 6**.
707
708 ***Structural modelling***
709 We utilized the AlphaFold 3 webserver (https://alphafoldserver.com) (*75*) to generate mono- and
710 tetrameric models. Each model was predicted using amino acid sequence of full-length MMF1 with
711 ADP (for monomer model) or with four ATP and four Mg^{2+} (for tetramer model), respectively. The

resulting models and RPP1 resistosome structure (PDB: 7CRC) were analyzed using ChimeraX version 1.8.

Statistical analysis

We used R (R core Team, 2016) for statistical analysis and visualization of data. The R version and package version used for each step of the analysis is documented at the end of the markdown files. All the code required to reproduce the statistical analysis and graphing can be found on the GitHub repository of this article. Figures were exported from R and combined and formatted using Adobe Illustrator. The appropriate statistical test used for each analysis is indicated in the corresponding figure legends and is annotated in the available code.

Data availability

We have deposited all source data together with all analysis scripts underlying all figures on GitHub (https://github.com/PMI-Basel/JansevanRensburg_et_al_GWAS_MMF1). The GitHub repository's structure follows the structure of this manuscript with separate folders of source data and analysis scripts on i) Accession growth feedback (Dataset 1), ii) MBOA sensitivity (Dataset 2), iii) GWAS statistics (Dataset 3), iv) Col-0 and mutant growth feedback (Dataset 4), v) microbiome (Dataset 5) and vi) transcriptome (Dataset 6). Each dataset and its analysis documentation (R-markdown outputs) is shared with this article as **Dataset 1** to **6** and the corresponding **Suppl. Files 1** to **6**. The raw sequencing data are stored at the European Nucleotide Archive (http://www.ebi.ac.uk/ena). The microbiome profiling is stored under project number PRJEB85607, the transcriptome data is available under PRJEB85599 and the genome of the *mmf1-2* mutant under PRJEB85789. The bioinformatic code of all analyses, including information on barcodes, primers and sample assignments is provided on GitHub. Raw images are available upon request.

Code availability

All the code required to reproduce the statistical analysis and graphing can be found on GitHub https://github.com/PMI-Basel/JansevanRensburg_et_al_GWAS_MMF1.

Acknowledgements

We specifically thank Nicolas Widmer from Agroscope Changins (Switzerland) for field access and assistance. We thank Prof. Jane Parker for providing Arabidopsis mutant seeds. We thank the team at the Plant Sciences Facility at Vienna BioCenter Core Facilities GmbH (VBCF), a member of the Vienna BioCenter (VBC), Austria, for their help with Arabidopsis image acquisition. We are very grateful to Dr. Pamela Nicholson and her team at the Next Generation Sequencing Platform in Bern for excellent technical support. We thank Dr. Phillipe Demougin and Dr. Christian Beisle (both University of Basel, Switzerland) for their support with RNAseq. Finally, we thank Duncan Crosbie (LMU Munich) and Helmut Blum and Stefan Krebs (Gene Center, LMU Munich) for support with genome sequencing of *mmf1-2*.

Funding

This project was funded by the Swiss National Foundation (Grant No. 189249 to K.S.), the Austrian Academy of Sciences (ÖAW, to C.B.), by the European Union's Horizon 2020 research and innovation programme by the European Research Council (ERC) (Grant Agreement No. 716823 'FEAR-SAP' to C.B.). N.S. received funding from the Deutsche Forschungsgemeinschaft (DFG) in the frame of TRR356 project A05 (project No. 491090170). H.A. received funding from the Japan Science and Technology Agency (JST), Precursory Research for Embryonic Science and Technology (Grant No. JPMJPR21D1) and Japan Society for the Promotion of Science (JSPS) (Grant No. 23K20042,

24H00010, 25K02012). For parts of the computational analyses, we used the BioHPC-Genomics compute cluster at the Leibniz Rechenzentrum Munich (DFG; grant no. 450674345) and the CLIP batch environment at the Vienna BioCenter.

Ethics declarations

None

Extended Data

Extended Data Figures: 1 - 9

Supplementary Materials

Figs. S1 to S2

Tables S1 to S3

Other Supplementary Materials for this manuscript include

Supplementary Files 1 – 6 (R markdowns with code to reproduce the analysis)

Datasets 1 – 6 (Datasets required for data analysis)

Extended Data

Title:

A TNL receptor mediates microbiome feedbacks in Arabidopsis

Authors:

Henry Janse van Rensburg[1*], Niklas Schandry[2,3*§], Jan Waelchli[1], Katja Stengele[1], Selma Cadot[1], Katharina Jandrasits[2], Hiroaki Adachi[4, 5], Claude Becker[2,3,§], Klaus Schlaeppi[1,§]

[1] Department of Environmental Sciences, University of Basel, Basel, Switzerland

[2] Gregor Mendel Institute of Molecular Plant Biology GmbH, Austrian Academy of Sciences, Vienna BioCenter (VBC), Vienna, Austria

[3] LMU Biocenter, Faculty of Biology, Ludwig-Maximilians-Universität Munich, Martinsried, Germany

[4] Graduate School of Agriculture, Kyoto University, Kyoto, Japan

[5] Faculty of Advanced Life Science, Hokkaido University, Sapporo, Japan

The file includes:

Extended figures.

Extended Data Figures 1 to 9

Extended Data

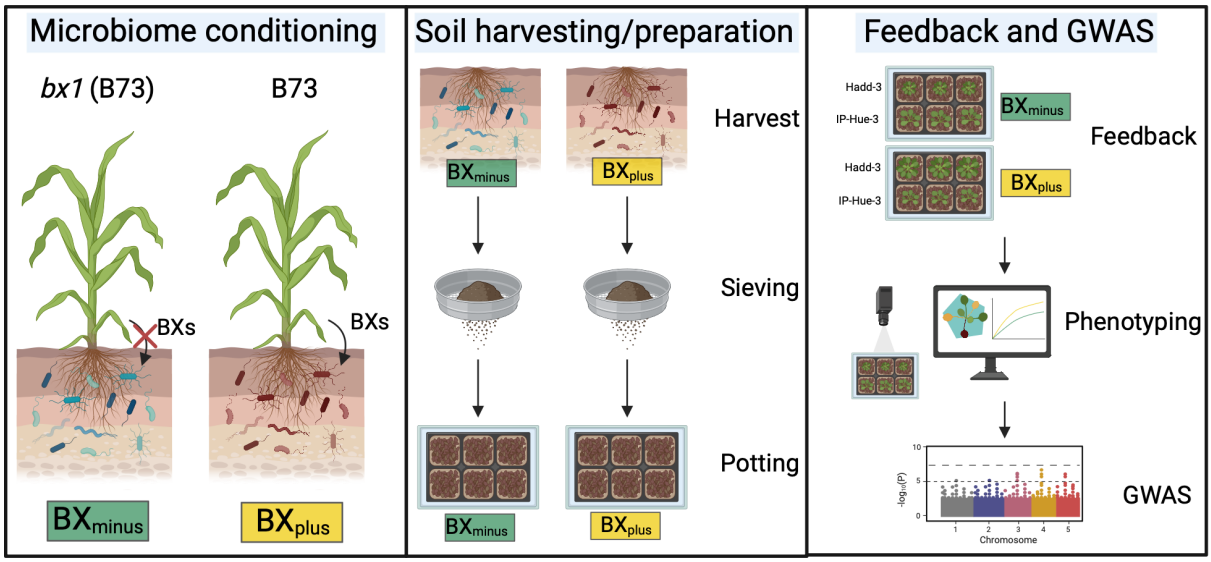

Extended Data Fig. 1. **Overview of the experimental workflow**. To condition the soil microbiomes, maize exuding BXs (B73) and a BX-deficient mutant (*bx1*) was grown for 12 weeks on field soil, resulting in a BX_{plus} and a BX_{minus} microbiome. The soil core surrounding the roots was removed and sieved to produce the soil used for growth-feedback assays. 410 Arabidopsis accessions were grown on the two conditioned soil microbiomes and phenotyped using a high-throughput phenotyping pipeline. Growth feedback response as the rosette size ($BX_{plus} - BX_{minus}$) on the two soil microbiomes was used as the phenotype for the genome-wide association study (GWAS). *Mediator of microbiome feedbacks 1* (*MMF1*) identified in the GWAS was functionally validated for growth feedback assays using T-DNA insertion mutant lines. The cause for lack of feedback in mutants were further dissected by analysing the microbiome and transcriptome of wild-type and mutant plants grown on the two microbiomes. Created with BioRender®.

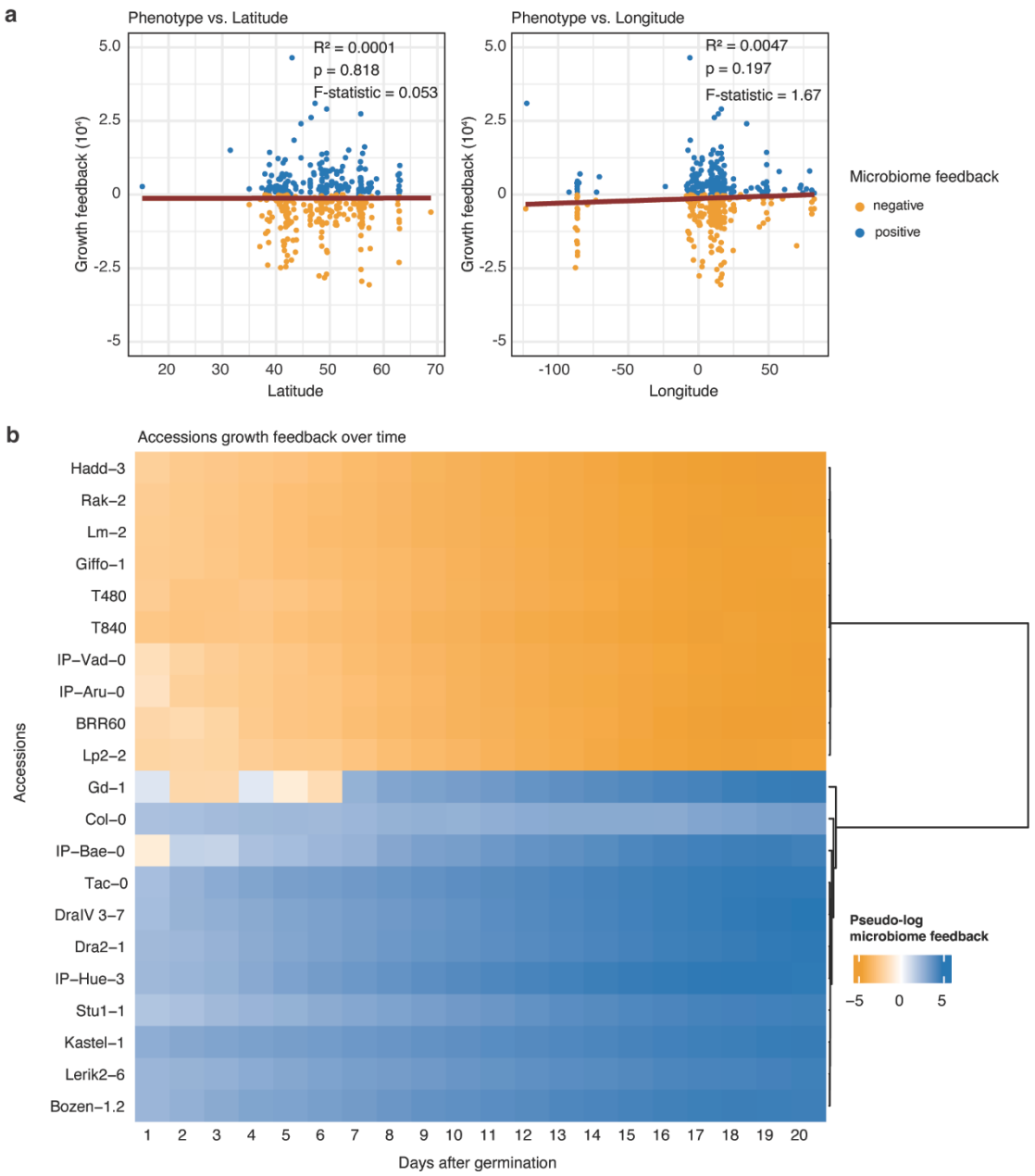

Extended Data Fig. 2. **Microbiome feedback of Arabidopsis accessions**. (**a**) Relationship between growth feedbacks and geographical location of the phenotyped accessions. Scatter plot illustrating the relationship between latitude or longitude and the microbiome feedback of accessions at 15 days after germination. Each data point is coloured according to its microbiome feedback response, with orange and blue denoting a negative or positive microbiome feedback, respectively. The plot includes a linear regression line (in red), highlighting the relationship between location and phenotype. The regression statistics, including the R-squared value (R^2) and the *p*-value of the F-test, are displayed in the top right corner of the plot. The R-squared value quantifies the proportion of variance in the phenotype explained by either latitude or longitude, while the *p*-value refers to testing the null hypothesis that the slope of the regression line is zero. (**b**) The daily microbiome feedback of Col-0 and the top 10 accessions with the strongest positive (blue) or negative (orange) BX-growth feedback when grown on the BX_{plus} and BX_{minus} soils. The heatmap colours are the pseudo-log transformed microbiome feedbacks (rosette area on BX_{plus} – rosette area on BX_{minus}). Accessions are clustered on the y-axis based on agglomerative hierarchical clustering using Ward's method performed using Dynamic Time Warping (DTW) distances and Ward's method to identify groups with similar response patterns over time. The dendrogram on the right side of the heat map illustrates the clustering structure, grouping accessions that exhibit similar trajectories in their growth feedback **Dataset 1**.

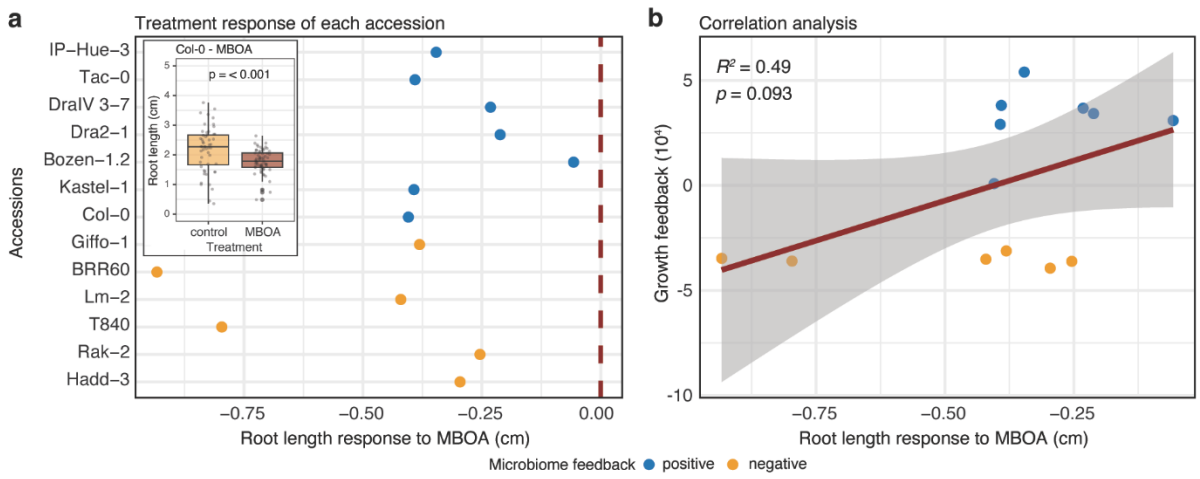

Extended Data Fig. 3. Direct allelopathic effect of benzoxazinoids on the growth of Arabidopsis. (**a**) Sensitivity to MBOA in terms of root length response (root length on control – root length on MBOA) of Col-0 and the accessions with the strongest positive or negative microbiome feedback. Accessions are colour-coded as to whether they showed a positive (blue) or negative (orange) microbiome feedback on the BX-conditioned soil microbiome in the GWAS experiment. Boxplot insert displays the root length of Col-0 on the control or MBOA treatment as an example. Plants were grown for 10 days on ½ MS media in the presence of 0.25 mM MBOA or control (DMSO). (**b**) Pearson's correlation analysis between MBOA sensitivity and microbiome feedback at 15 days after germination across the different accessions. The scatter plot displays individual data points coloured by microbiome feedback, with positive responses shown in blue and negative responses in orange. A linear regression line (in red) illustrates the trend between the two variables. The correlation coefficient (R^2) and p-value are annotated on the plot, indicating the strength and statistical probability of the relationship. **Dataset 2.**

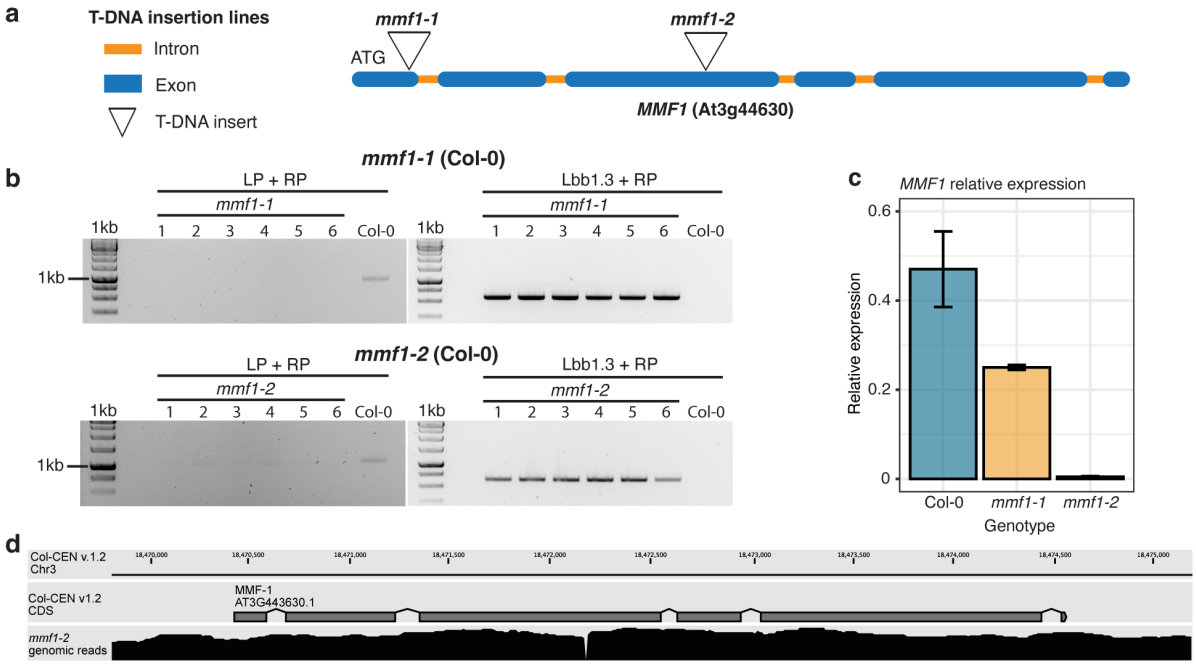

Extended Data Fig. 4. **Genetic characterization of *mmf1* T-DNA insertion lines.** (**a**) Genomic location of the T-DNA insertion sites for *mmf1-1* and *mmf1-2* in the open reading frame of *MMF1*. Exons and introns are shown in colour, and the T-DNA insertion position as triangles. (**b**) Genotyping results of *mmf1-1* (SALK_144159C) and *mmf1-2* (SALK_002318C) by PCR to confirm the presence of the T-DNA insertion. The gels represent genotyping of 6 mutant plants for the T-DNA insertion allele (left, LBb1.3 and RP primers) and the wild-type allele (right, LP and RP primers). (**c**) Relative expression levels of *MMF1* determined by qRT-PCR in wild-type (Col-0) and the two *MMF1* mutant lines. (**d**) Mapping of genomic long-reads from *mmf1-2* onto Col-CEN v1.2. Top panel shows the genomic coordinates on chromosome 3, middle panel shows the annotation of the coding sequence of *mmf-1,* bottom panel shows the aggregated pile-up of mapped reads, confirming the T-DNA insertion in the third exon.

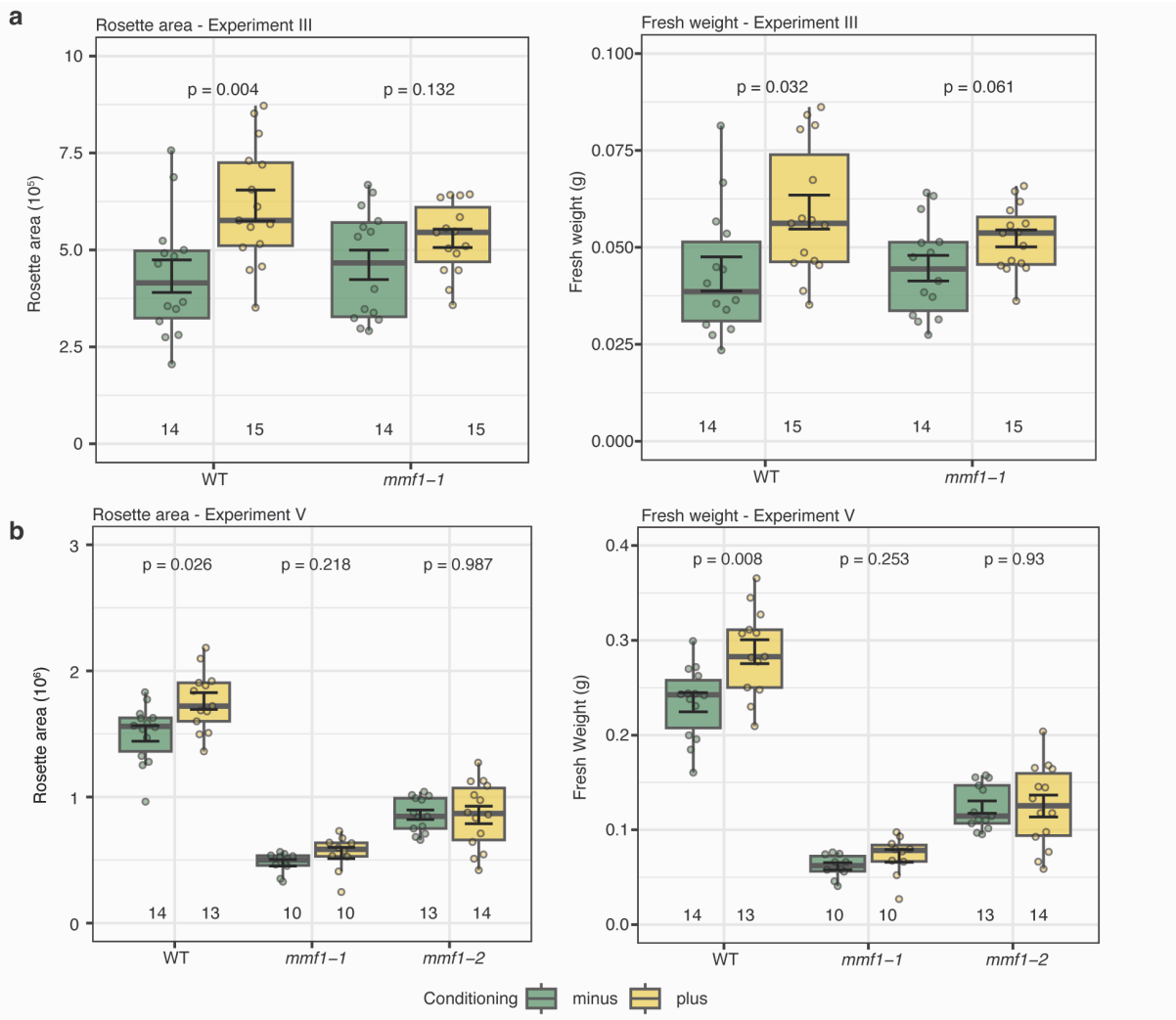

c

LLM and EMM - Rosette Area
[weight ~ genotype * microbiome + (1 | experiment)]

	Estimate	*P*
LMM		
WT:microbiome	1.6×10^5	0.023
mmf1-1:BX+ effect	-1.2×10^5	0.250
mmf1-2:BX+ effect	-1.7×10^5	0.089
EMM		
WT (BX+ – BX-)	1.6×10^5	0.024
mmf1-1 (BX+ – BX-)	4.1×10^4	0.587
mmf1-2 (BX+ – BX-)	9.6×10^3	0.891

LLM and EMM - Weight
[weight ~ genotype * microbiome + (1 | experiment)]

	Estimate	*P*
LMM		
WT:microbiome	0.036	< 0.001
mmf1-1:BX+ effect	-0.030	0.055
mmf1-2:BX+ effect	-0.032	0.033
EMM		
WT (BX+ – BX-)	0.036	< 0.001
mmf1-1 (BX+ – BX-)	0.006	0.583
mmf1-2 (BX+ – BX-)	0.004	0.698

Extended Data Fig. 5. Growth feedback in a BX_{plus} microbiome is consistently lost in *mmf1* mutants. (**a** and **b**) Repeated growth feedbacks (Experiment II and IV) of Col-0 wild-type (WT) and two *mmf1* T-DNA insertion mutants (*At3g44630*) grown on the BX_{minus} and BX_{plus} soil microbiomes. Feedback experiments were performed on greenhouse-conditioned soil batches (**a**) BS04 and (**b**) BS09. Graphs illustrate the rosette area (in pixels) of 6-week-old plants. Sample sizes are indicated at the bottom of each plot. Output of the ANOVA and FDR corrected *p*-values are indicated in each plot. (**c**) A linear mixed-effects model and estimate marginal means (fresh weight/rosette area ~ line * BX + (1 | experiment)) was used to assess the effects of plant genotype (line), on the growth response to the two microbiomes, with experiment included as a random effect. Data from experiment V and VI were included in the model. **Dataset 4.**

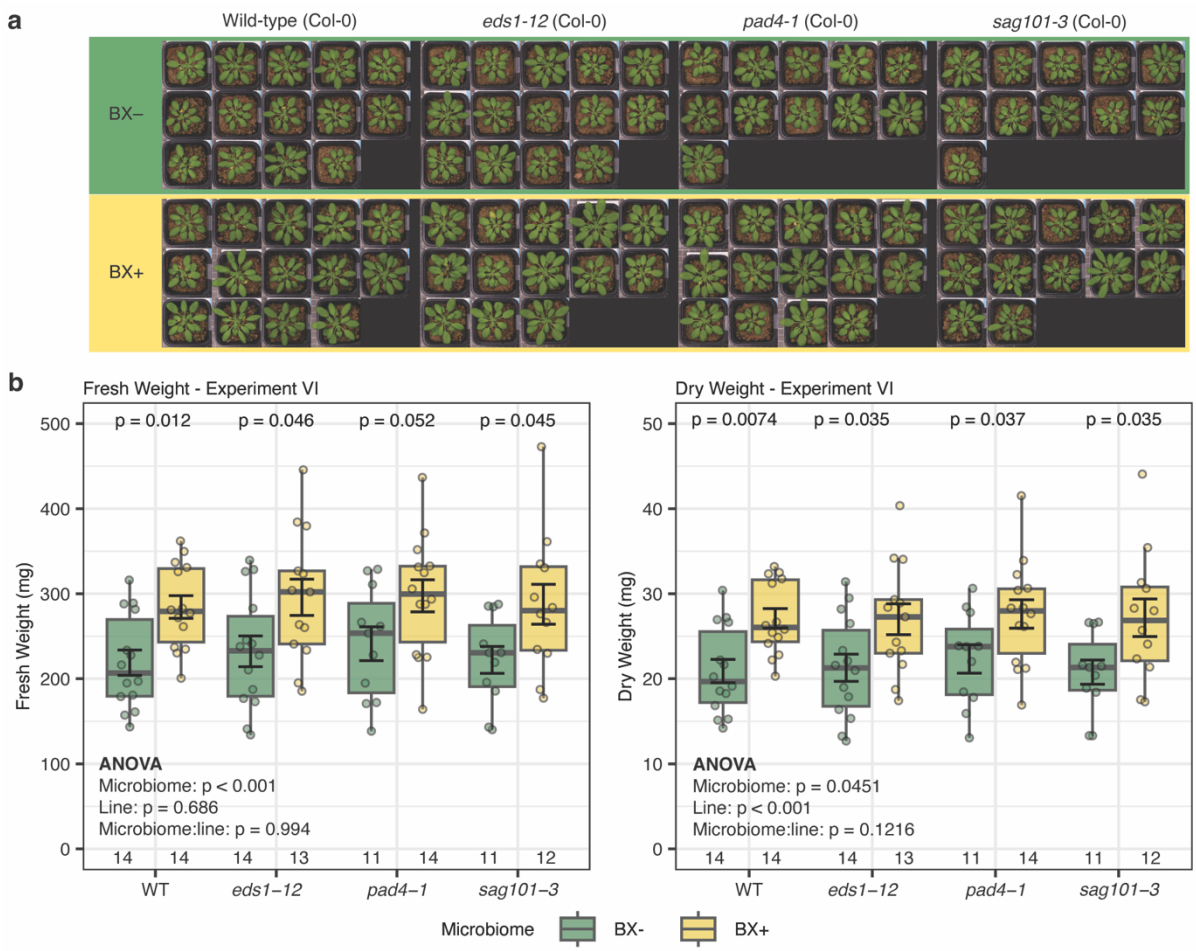

Extended Data Fig. 6. Growth feedback in a BX_{plus} microbiome remains intact in effector-triggered immunity signalling mutants. (**a**) Phenotypes of 6-week-old WT, and mutants (*eds1-12*, *pad4-1* and *sag101-3*) affected in effector-triggered immunity signalling pathways grown on the BX_{minus} and BX_{plus} soils. (**b**) Fresh weight, and dry weight of WT, *eds1-12*, *pad4-1* and *sag101-3* illustrate the positive growth feedback on the BX_{plus} soil microbiome. Boxplots illustrate the median, standard error, and interquartile range, and the whiskers extend from the box to the smallest and largest values. Sample numbers are indicated at the bottom of each plot. ANOVA output and FDR-corrected *p*-values comparing the growth feedback of each line are shown above the graph. **Dataset 4.**

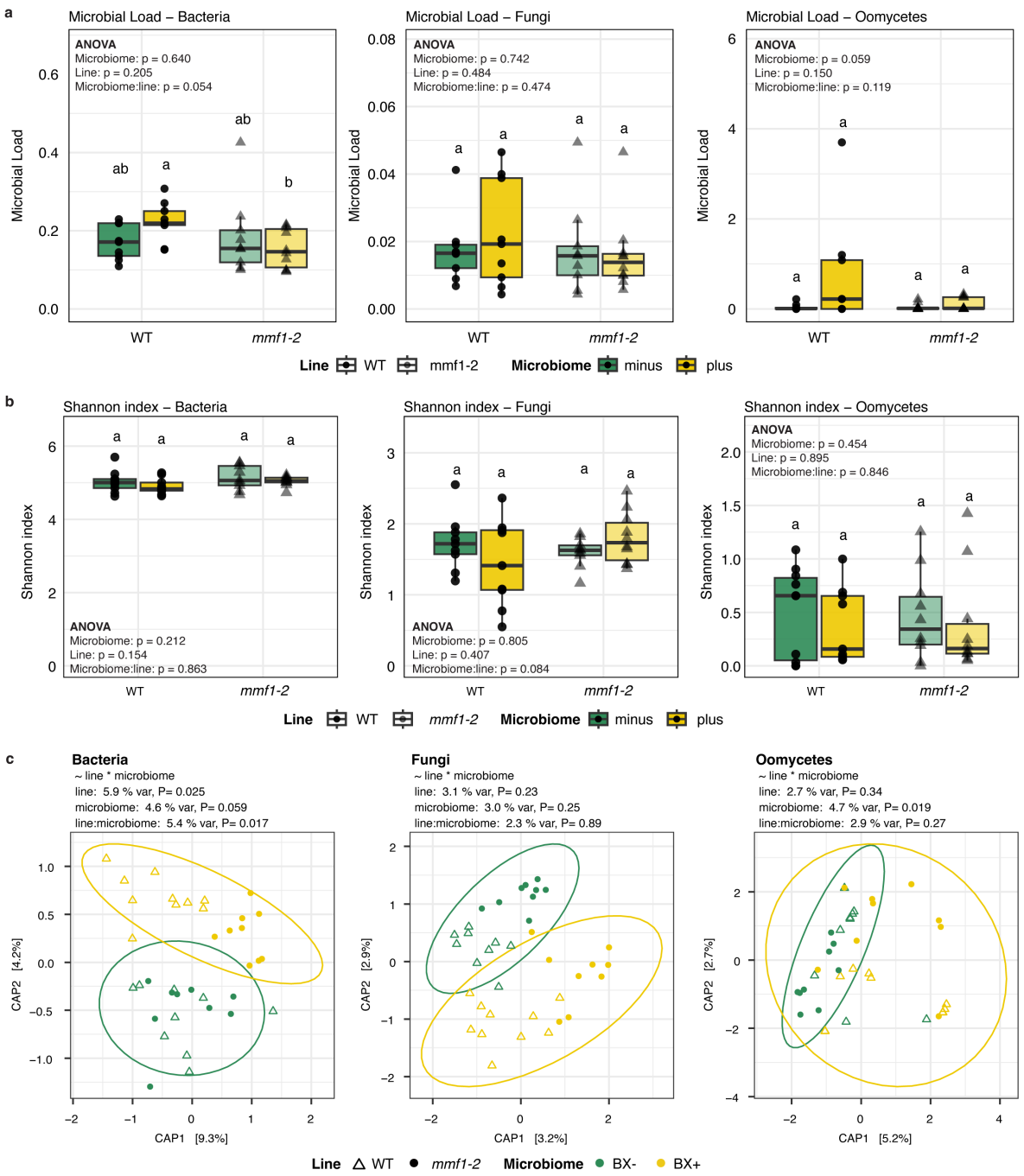

Extended Data Fig. 7. Root microbiota profiling of WT and *mmf1-2* mutants grown on the BX_{minus} or BX_{minus} soils. (**a**) Bacterial, fungal and oomycete load in the roots of wild-type (WT) and mmf1-2 mutants grown on BX_{plus} and BX_{minus} soil. Bacterial load calculated by dividing microbial abundance by host abundance (GIGANTEA). Comparisons between the two lines are shown as *p*-values based on Kruskal-Wallis Test. (**b**) Microbial richness in the roots of the same plants grown on the two soils displayed as Shannon indices. Individual samples are shown as dots. Comparisons between the two lines are shown as *p*-values based on Kruskal-Wallis Test. (**c**) The output of PERMANOVA on Bray-Curtis dissimilarities of the bacterial, fungal and oomycete root microbiota of Arabidopsis WT (filled circles) and *mmf1-2* mutants (open triangles) grown on the BX_{minus} (green) and BX_{plus} (yellow) soils. The R^2 and *p* values indicate the line and conditioning effect and their interaction on the two soils. Constrained Analysis of Principal Coordinates (CAP) visually illustrating the effects found in the PERMANOVA analysis. Plants grown on a BX_{plus} (yellow) and BX_{minus} (green) soil microbiome are grouped based on a 95% confidence interval. The axes show the percentage of explained variance for the first two principal components.

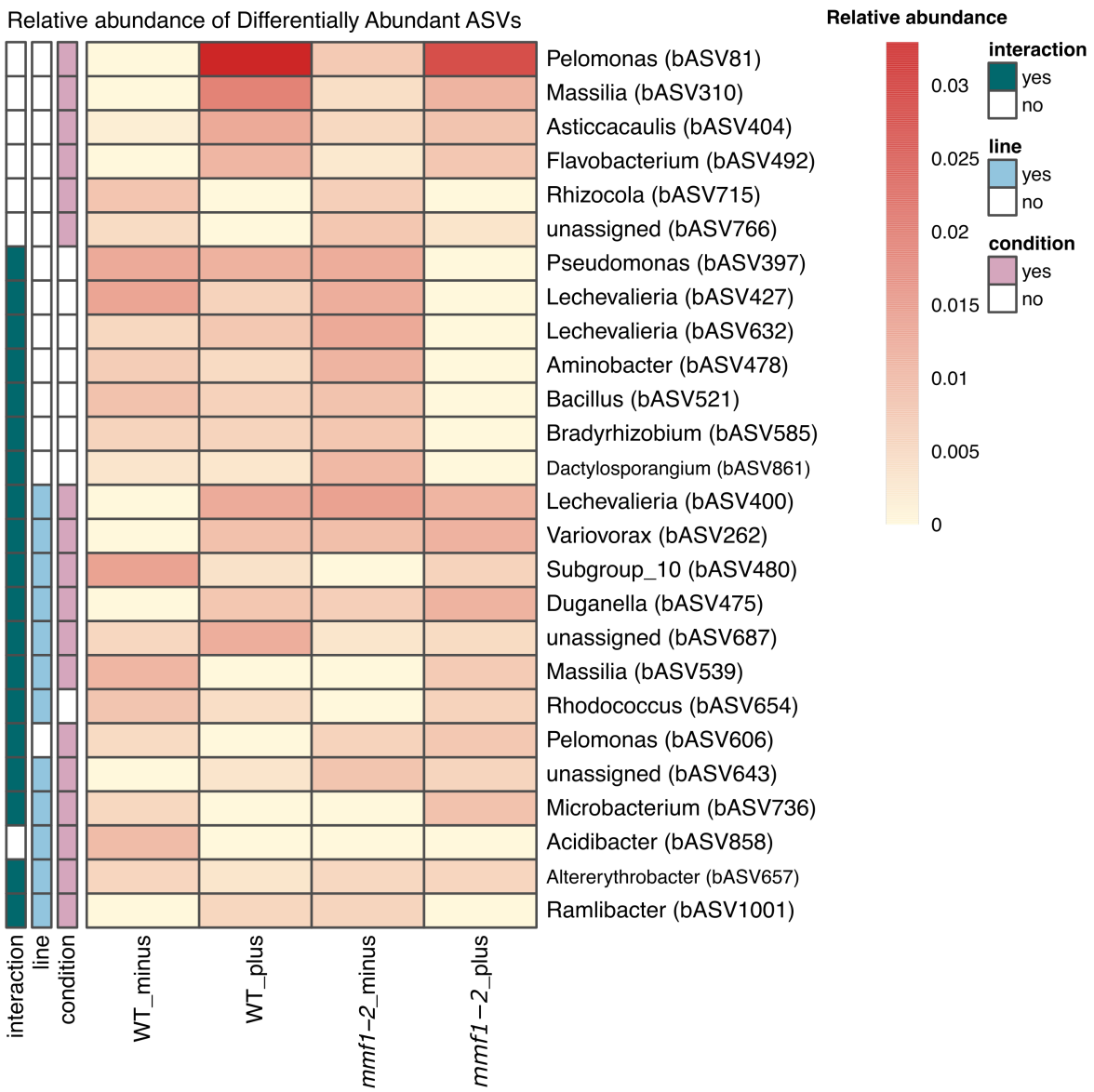

Extended Data Fig. 8. Relative abundances of differentially abundant ASVs in the roots of wild-type and *mmf1* mutants. Square-root-transformed relative abundances of differentially abundant ASVs in the roots of wild-type and *mmf1-2* mutant plants grown on the BX_{minus} or BX_{plus} soil microbiomes. Differential abundance was assessed using DESeq2 with a full factorial model including genotype (*line*), microbiome (*condition*), and their interaction. ASVs were considered significant if they had an absolute $\log_2$ fold change ≥ 1 and a false discovery rate (FDR) < 0.05. Significant ASVs were grouped by the model term(s) they were associated with: condition (pink), genotype (light blue), or interaction (green). Within each group, ASVs are sorted by their average abundance. Genus-level taxonomic annotations are shown, and in parentheses the ASV IDs.

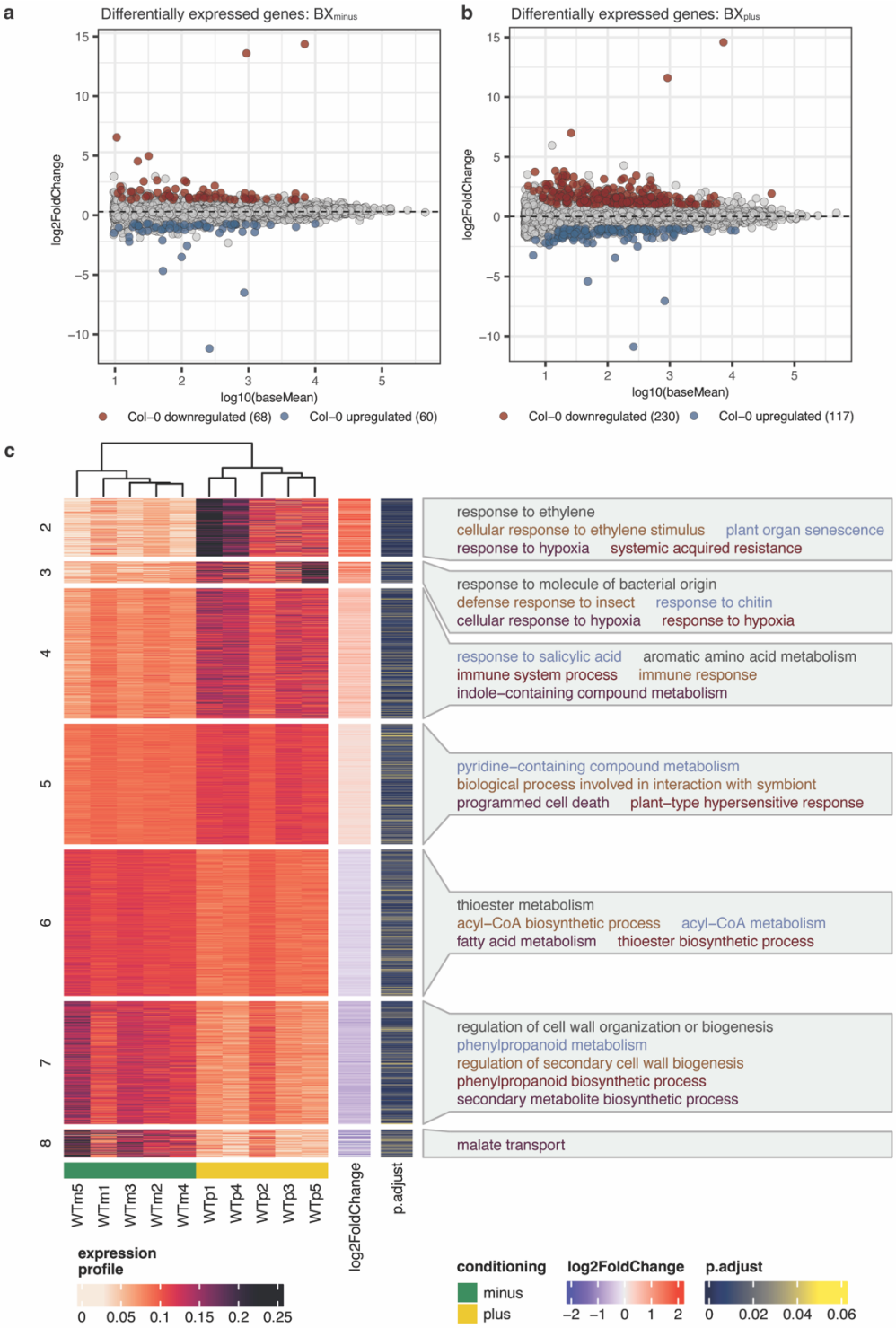

Extended Data Fig. 9. Root transcriptome of WT and *mmf1-2* mutants grown on the BX_{minus} and BX_{plus} soils. MA plot of differentially expressed genes between *mmf1-2* mutants and WT plants in response to the (**a**) BX_{minus} and (**b**) BX_{plus} soil microbiome. Significantly differentially expressed genes were calculated using DESeq2 (log_2fold change ≥ 1; empirical Bayes statistic false discovery rate < 0.05). (**c**) Heatmap showing the co-expressed gene clusters (Benjamini-Hochberg-correction, p-adjust < 0.01) as identified by coseq for plants grown on BX_{minus} (green) or BX_{plus} (yellow) soils. Colours of the heatmap indicates the expression profiles in terms of normalized gene counts for each gene. The log2Fold change and adjusted *p* values (empirical Bayes shrinking) for each gene inferred from DESeq2 is shown on the right. Cluster labels show the top 5 enriched GO terms for biological function within each cluster. GO text colour is for better readability only. Full tables of all enriched GO terms in each cluster are provided in **Dataset 6**.

References

1. P. Trivedi, J. E. Leach, S. G. Tringe, T. Sa, B. K. Singh, Plant–microbiome interactions: from community assembly to plant health. *Nature Reviews Microbiology* **18**, 607–621 (2020).

2. R. L. Berendsen, C. M. J. Pieterse, P. A. H. M. Bakker, The rhizosphere microbiome and plant health. *Trends in Plant Science* **17**, 478–486 (2012).

3. R. Mendes, P. Garbeva, J. M. Raaijmakers, The rhizosphere microbiome: Significance of plant beneficial, plant pathogenic, and human pathogenic microorganisms. *FEMS Microbiology Reviews* **37**, 634–663 (2013).

4. W.-J. Li, X.-Y. Zhou, X.-L. An, L.-J. Li, C.-S. Lin, H. Li, H.-Z. Li, Enhancement of beneficial microbiomes in plant–soil continuums through organic fertilization: Insights into the composition and multifunctionality. *Soil Ecol. Lett.* **6**, 230223 (2024).

5. H. Janse van Rensburg, K. Stengele, K. Schlaeppi, Understanding plant responsiveness to microbiome feedbacks. *Current Opinion in Plant Biology* **81**, 102603 (2024).

6. T. M. Bezemer, C. S. Lawson, K. Hedlund, A. R. Edwards, A. J. Brook, J. M. Igual, S. R. Mortimer, W. H. Van Der Putten, Plant species and functional group effects on abiotic and microbial soil properties and plant-soil feedback responses in two grasslands. *Journal of Ecology* **94**, 893–904 (2006).

7. W. H. Van der Putten, R. D. Bardgett, J. D. Bever, T. M. Bezemer, B. B. Casper, T. Fukami, P. Kardol, J. N. Klironomos, A. Kulmatiski, J. A. Schweitzer, K. N. Suding, T. F. J. Van de Voorde, D. A. Wardle, Plant-soil feedbacks: The past, the present and future challenges. *Journal of Ecology* **101**, 265–276 (2013).

8. M. A. Meier, G. Xu, M. G. Lopez-Guerrero, G. Li, C. Smith, B. Sigmon, J. R. Herr, J. R. Alfano, Y. Ge, J. C. Schnable, J. Yang, Association analyses of host genetics, root-colonizing microbes, and plant phenotypes under different nitrogen conditions in maize. *eLife* **11** (2022).

9. Y. Song, E. Atza, J. J. S. Gil, D. Akkermans, R. de Jonge, P. G. H. de Rooij, D. Kakembo, P. A. H. M. Bakker, C. M. J. Pieterse, N. V. Budko, R. L. Berendsen, Seed tuber microbiome is a predictor of next-season potato vigor. *bioRxiv*, 2024.04.18.590071 (2024).

10. M. Wang, A.-H. Ge, X. Ma, X. Wang, Q. Xie, L. Wang, X. Song, M. Jiang, W. Yang, J. D. Murray, Y. Wang, H. Liu, X. Cao, E. Wang, Dynamic root microbiome sustains soybean productivity under unbalanced fertilization. *Nat Commun* **15**, 1668 (2024).

11. R. C. Wilhelm, H. M. van Es, D. H. Buckley, Predicting measures of soil health using the microbiome and supervised machine learning. *Soil Biology and Biochemistry* **164**, 108472 (2022).

939 12. X. Qiao, S. Bei, G. Wang, C. Li, H. Li, J. Zhang, F. Zhang, Soil biota is decisive for
940 overyielding in intercropping under low phosphorus conditions. *Journal of Applied*
941 *Ecology* **59**, 1804–1814 (2022).

942 13. M. Chialva, A. Salvioli di Fossalunga, S. Daghino, S. Ghignone, P. Bagnaresi, M.
943 Chiapello, M. Novero, D. Spadaro, S. Perotto, P. Bonfante, Native soils with their
944 microbiotas elicit a state of alert in tomato plants. *New Phytologist* **220** (2018).

945 14. L. Hu, C. A. M. Robert, S. Cadot, X. Zhang, M. Ye, B. Li, D. Manzo, N. Chervet, T.
946 Steinger, M. G. A. Van Der Heijden, K. Schlaeppi, M. Erb, Root exudate metabolites
947 drive plant-soil feedbacks on growth and defense by shaping the rhizosphere
948 microbiota. *Nature Communications* **9**, 1–13 (2018).

949 15. P. J. P. Teixeira, N. R. Colaianni, C. R. Fitzpatrick, J. L. Dangl, Beyond pathogens:
950 microbiota interactions with the plant immune system. *Current Opinion in*
951 *Microbiology* **49**, 7–17 (2019).

952 16. K. Yu, C. M. J. Pieterse, P. A. H. M. Bakker, R. L. Berendsen, Beneficial microbes going
953 underground of root immunity. *Plant, Cell & Environment* **42**, 2860 (2019).

954 17. J. Bergelson, J. Mittelstrass, M. W. Horton, Characterizing both bacteria and fungi
955 improves understanding of the Arabidopsis root microbiome. *Scientific Reports 2019*
956 *9:1* **9**, 1–11 (2019).

957 18. M. Hu, J.-M. Zhou, Research on ADR1s helps understanding the plant immune network.
958 *Stress Biology* **2**, 12 (2022).

959 19. J. Bigeard, J. Colcombet, H. Hirt, Signaling mechanisms in pattern-triggered immunity
960 (PTI). *Molecular Plant* **8**, 521–539 (2015).

961 20. F. Locci, J. E. Parker, Plant NLR immunity activation and execution: a biochemical
962 perspective. *Open Biology* **14** (2024).

963 21. F. Monteiro, M. T. Nishimura, Structural, functional, and genomic diversity of plant NLR
964 proteins: An evolved resource for rational engineering of plant immunity. *Annual*
965 *Review of Phytopathology* **56**, 243–267 (2018).

966 22. G. Castrillo, P. J. P. L. Teixeira, S. H. Paredes, T. F. Law, L. De Lorenzo, M. E. Feltcher, O.
967 M. Finkel, N. W. Breakfield, P. Mieczkowski, C. D. Jones, J. Paz-Ares, J. L. Dangl, Root
968 microbiota drive direct integration of phosphate stress and immunity. *Nature* **543**,
969 513–518 (2017).

970 23. S. L. Lebeis, S. H. Paredes, D. S. Lundberg, N. Breakfield, J. Gehring, M. McDonald, S.
971 Malfatti, T. G. Del Rio, C. D. Jones, S. G. Tringe, J. L. Dangl, Salicylic acid modulates
972 colonization of the root microbiome by specific bacterial taxa. *Science* **349**, 860–864
973 (2015).

24. S. Pfeilmeier, G. C. Petti, M. Bortfeld-Miller, B. Daniel, C. M. Field, S. Sunagawa, J. A. Vorholt, The plant NADPH oxidase RBOHD is required for microbiota homeostasis in leaves. *Nature Microbiology* **6**, 852–864 (2021).

25. M. Frey, K. Schullehner, R. Dick, A. Fiesselmann, A. Gierl, Benzoxazinoid biosynthesis, a model for evolution of secondary metabolic pathways in plants. *Phytochemistry* **70**, 1645–1651 (2009).

26. S. Cadot, H. Guan, M. Bigalke, J. C. Walser, G. Jander, M. Erb, M. G. A. van der Heijden, K. Schlaeppi, Specific and conserved patterns of microbiota-structuring by maize benzoxazinoids in the field. *Microbiome* **9**, 1–19 (2021).

27. T. E. A. Cotton, P. Pétriacq, D. D. Cameron, M. A. Meselmani, R. Schwarzenbacher, S. A. Rolfe, J. Ton, Metabolic regulation of the maize rhizobiome by benzoxazinoids. *ISME Journal* **13**, 1647–1658 (2019).

28. S. Cadot, V. Gfeller, L. Hu, N. Singh, A. Sánchez-Vallet, G. Glauser, D. Croll, M. Erb, M. G. A. van der Heijden, K. Schlaeppi, Soil composition and plant genotype determine benzoxazinoid-mediated plant–soil feedbacks in cereals. *Plant Cell and Environment* **44**, 3502–3514 (2021).

29. V. Gfeller, J. Waelchli, S. Pfister, G. Deslandes-Hérold, F. Mascher, G. Glauser, Y. Aeby, A. Mestrot, C. A. M. Robert, K. Schlaeppi, M. Erb, Plant secondary metabolite-dependent plant-soil feedbacks can improve crop yield in the field. *eLife* **12** (2023).

30. K. Stengele, L. Stauber, L. Thoenen, H. Janse van Rensburg, V. D'Adda, K. Schlaeppi, Benzoxazinoid-mediated microbiome feedbacks enhance Arabidopsis growth and defense. bioRxiv [Preprint] (2024). https://doi.org/10.1101/2024.10.21.619081.

31. A. Martinez-Medina, V. Flors, M. Heil, B. Mauch-Mani, C. M. J. Pieterse, M. J. Pozo, J. Ton, N. M. van Dam, U. Conrath, Recognizing Plant Defense Priming. *Trends in Plant Science* **21**, 818–822 (2016).

32. H. Yue, X. Sun, T. Wang, A. Zhang, D. Han, G. Wei, W. Song, D. Shu, Host genotype-specific rhizosphere fungus enhances drought resistance in wheat. *Microbiome* **12**, 1–19 (2024).

33. P. C. A. Wintermans, P. A. H. M. Bakker, C. M. J. Pieterse, Natural genetic variation in Arabidopsis for responsiveness to plant growth-promoting rhizobacteria. *Plant Molecular Biology* **90**, 623–634 (2016).

34. The 1001 Genomes Consortium, 1,135 Genomes Reveal the Global Pattern of Polymorphism in Arabidopsis thaliana. *Cell* **166**, 481–491 (2016).

35. P. Hüther, N. Schandry, K. Jandrasits, I. Bezrukov, C. Becker, ARADEEPOPSIS, an automated workflow for top-view plant phenomics using semantic segmentation of leaf States. *Plant Cell* **32**, 3674–3688 (2020).

1010 36. R. G. Belz, K. Hurle, Differential exudation of two benzoxazinoids - One of the
1011 determining factors for seedling allelopathy of Triticeae species. *Journal of Agricultural*
1012 *and Food Chemistry* **53**, 250–261 (2005).

1013 37. N. Schandry, C. Becker, Allelopathic Plants: Models for Studying Plant–Interkingdom
1014 Interactions. *Trends in Plant Science* **25**, 176–185 (2020).

1015 38. V. Gfeller, S. Cadot, J. Waelchli, S. Gulliver, C. Terrettaz, L. Thönen, P. Mateo, C. A. M.
1016 Robert, F. Mascher, T. Steinger, M. Bigalke, M. Erb, K. Schlaeppi, Soil chemical and
1017 microbial gradients determine accumulation of root-exuded secondary metabolites
1018 and plant–soil feedbacks in the field. *Journal of Sustainable Agriculture and*
1019 *Environment* **2**, 173–188 (2023).

1020 39. C. Lippert, F. P. Casale, B. Rakitsch, O. Stegle, LIMIX: genetic analysis of multiple traits.
1021 doi: 10.1101/003905 (2014).

1022 40. S. Ma, D. Lapin, L. Liu, Y. Sun, W. Song, X. Zhang, E. Logemann, D. Yu, J. Wang, J.
1023 Jirschitzka, Z. Han, P. Schulze-Lefert, J. E. Parker, J. Chai, Direct pathogen-induced
1024 assembly of an NLR immune receptor complex to form a holoenzyme. *Science* **370**,
1025 eabe3069 (2020).

1026 41. J. A. Dongus, J. E. Parker, EDS1 signalling: At the nexus of intracellular and surface
1027 receptor immunity. *Current Opinion in Plant Biology* **62**, 102039 (2021).

1028 42. J. Ordon, J. Gantner, J. Kemna, L. Schwalgun, M. Reschke, J. Streubel, J. Boch, J.
1029 Stuttmann, Generation of chromosomal deletions in dicotyledonous plants employing
1030 a user-friendly genome editing toolkit. *Plant Journal* **89**, 155–168 (2017).

1031 43. R. N. Pruitt, F. Locci, F. Wanke, L. Zhang, S. C. Saile, A. Joe, D. Karelina, C. Hua, K.
1032 Fröhlich, W. L. Wan, M. Hu, S. Rao, S. C. Stolze, A. Harzen, A. A. Gust, K. Harter, M. H. A.
1033 J. Joosten, B. P. H. J. Thomma, J. M. Zhou, J. L. Dangl, D. Weigel, H. Nakagami, C.
1034 Oecking, F. E. Kasmi, J. E. Parker, T. Nürnberger, The EDS1–PAD4–ADR1 node mediates
1035 Arabidopsis pattern-triggered immunity. *Nature* **598**, 495–499 (2021).

1036 44. D. S. Lundberg, P. P. N. Ayutthaya, A. Strauß, G. Shirsekar, W. S. Lo, T. Lahaye, D.
1037 Weigel, Host-associated microbe pcr (Hampcr) enables convenient measurement of
1038 both microbial load and community composition. *eLife* **10** (2021).

1039 45. M. I. Love, W. Huber, S. Anders, Moderated estimation of fold change and dispersion
1040 for RNA-seq data with DESeq2. *Genome Biology* **15**, 550 (2014).

1041 46. J. Lang, B. Genot, J. Bigeard, J. Colcombet, MPK3 and MPK6 control salicylic acid
1042 signaling by up-regulating *NLR* receptors during pattern- and effector-triggered
1043 immunity. *Journal of Experimental Botany* **73**, 2190–2205 (2022).

1044 47. T. Chen, K. Nomura, X. Wang, R. Sohrabi, J. Xu, L. Yao, B. C. Paasch, L. Ma, J. Kremer, Y.
1045 Cheng, L. Zhang, N. Wang, E. Wang, X. F. Xin, S. Y. He, A plant genetic network for
1046 preventing dysbiosis in the phyllosphere. *Nature* **580**, 653–657 (2020).

1047 48. P. Runge, “Structural variation of a polymorphic RPP1-like cluster in local Arabidopsis
1048 thaliana populations alters phyllosphere microbiome in Gorzów Wielkopolski,” thesis,
1049 University of Tübingen, Germany (2022).

1050 49. S. Goritschnig, A. D. Steinbrenner, D. J. Grunwald, B. J. Staskawicz, Structurally distinct
1051 Arabidopsis thaliana NLR immune receptors recognize tandem WY domains of an
1052 oomycete effector. *New Phytologist* **210**, 984–996 (2016).

1053 50. D. Maag, A. Köhler, C. A. M. Robert, M. Frey, J. L. Wolfender, T. C. J. Turlings, G.
1054 Glauser, M. Erb, Highly localized and persistent induction of Bx1-dependent herbivore
1055 resistance factors in maize. *The Plant Journal* **88**, 976–991 (2016).

1056 51. D. Jirage, T. L. Tootle, T. L. Reuber, L. N. Frost, B. J. Feys, J. E. Parker, F. M. Ausubel, J.
1057 Glazebrook, Arabidopsis thaliana PAD4 encodes a lipase-like gene that is important for
1058 salicylic acid signaling. *Proceedings of the National Academy of Sciences* **96**, 13583–
1059 13588 (1999).

1060 52. X. Sun, D. Lapin, J. M. Feehan, S. C. Stolze, K. Kramer, J. A. Dongus, J. Rzemieniewski, S.
1061 Blanvillain-Baufumé, A. Harzen, J. Bautor, P. Derbyshire, F. L. H. Menke, I. Finkemeier,
1062 H. Nakagami, J. D. G. Jones, J. E. Parker, Pathogen effector recognition-dependent
1063 association of NRG1 with EDS1 and SAG101 in TNL receptor immunity. *Nat Commun*
1064 **12**, 3335 (2021).

1065 53. C. Cardoso, T. Charnikhova, M. Jamil, P. M. Delaux, F. Verstappen, M. Amini, D.
1066 Lauressergues, C. Ruyter-Spira, H. Bouwmeester, Differential activity of Striga
1067 hermonthica seed germination stimulants and Gigaspora rosea hyphal branching
1068 factors in rice and their contribution to underground communication. *PLoS ONE* **9**
1069 (2014).

1070 54. M. Togninalli, Ü. Seren, D. Meng, J. Fitz, M. Nordborg, D. Weigel, K. Borgwardt, A.
1071 Korte, D. G. Grimm, The AraGWAS Catalog: A curated and standardized Arabidopsis
1072 thaliana GWAS catalog. *Nucleic Acids Research* **46**, D1150–D1156 (2018).

1073 55. Á. Ferrero-Serrano, S. M. Assmann, Phenotypic and genome-wide association with the
1074 local environment of Arabidopsis. *Nature Ecology and Evolution* **3**, 274–285 (2019).

1075 56. M. Kolmogorov, J. Yuan, Y. Lin, P. A. Pevzner, Assembly of long, error-prone reads using
1076 repeat graphs. *Nat Biotechnol* **37**, 540–546 (2019).

1077 57. M. Naish, M. Alonge, P. Wlodzimierz, A. J. Tock, B. W. Abramson, A. Schmücker, T.
1078 Mandáková, B. Jamge, C. Lambing, P. Kuo, N. Yelina, N. Hartwick, K. Colt, L. M. Smith, J.
1079 Ton, T. Kakutani, R. A. Martienssen, K. Schneeberger, M. A. Lysak, F. Berger, A. Bousios,
1080 T. P. Michael, M. C. Schatz, I. R. Henderson, The genetic and epigenetic landscape of
1081 the Arabidopsis centromeres. *Science* **374**, eabi7489 (2021).

1082 58. M. Alonge, L. Lebeigle, M. Kirsche, K. Jenike, S. Ou, S. Aganezov, X. Wang, Z. B.
1083 Lippman, M. C. Schatz, S. Soyk, Automated assembly scaffolding using RagTag elevates
1084 a new tomato system for high-throughput genome editing. *Genome Biology* **23**, 258
1085 (2022).

1086 59. A. Shumate, S. L. Salzberg, Liftoff: accurate mapping of gene annotations.
1087 *Bioinformatics* **37**, 1639–1643 (2021).

1088 60. M. Narusaka, T. Shiraishi, M. Iwabuchi, Y. Narusaka, The floral inoculating protocol: a
1089 simplified Arabidopsis thaliana transformation method modified from floral dipping.
1090 *Plant Biotechnology* **27**, 349–351 (2010).

1091 61. E. Knoch, J. Kovács, S. Deiber, R. Shanmuganathan, N. Serra Serra, C. Becker, N.
1092 Schandry, N. Serra, S. C. Becker, Transcriptional response of a target plant to
1093 benzoxazinoid and diterpene allelochemicals highlights commonalities in
1094 detoxification. *bioRxiv*, 2022.02.21.480921 (2022).

1095 62. C. A. Schneider, W. S. Rasband, K. W. Eliceiri, NIH Image to ImageJ: 25 years of Image
1096 Analysis. *Nat Methods* **9**, 671–675 (2012).

1097 63. Y. Bai, D. B. Müller, G. Srinivas, R. Garrido-Oter, E. Potthoff, M. Rott, N. Dombrowski, P.
1098 C. Münch, S. Spaepen, M. Remus-Emsermann, B. Hüttel, A. C. McHardy, J. A. Vorholt, P.
1099 Schulze-Lefert, Functional overlap of the Arabidopsis leaf and root microbiota. *Nature*
1100 *2015 528:7582* **528**, 364–369 (2015).

1101 64. K. L. McGuire, S. G. Payne, M. I. Palmer, C. M. Gillikin, D. Keefe, S. J. Kim, S. M.
1102 Gedallovich, J. Discenza, R. Rangamannar, J. A. Koshner, A. L. Massmann, G. Orazi, A.
1103 Essene, J. W. Leff, N. Fierer, Digging the New York City Skyline: Soil Fungal Communities
1104 in Green Roofs and City Parks. *PLOS ONE* **8**, e58020 (2013).

1105 65. M. Martin, Cutadapt removes adapter sequences from high-throughput sequencing
1106 reads. *EMBnet.journal* **17**, 10 (2011).

1107 66. B. J. Callahan, P. J. McMurdie, M. J. Rosen, A. W. Han, A. J. A. Johnson, S. P. Holmes,
1108 DADA2: High-resolution sample inference from Illumina amplicon data. *Nature*
1109 *Methods* **13**, 581–583 (2016).

1110 67. C. Quast, E. Pruesse, P. Yilmaz, J. Gerken, T. Schweer, P. Yarza, J. Peplies, F. O. Glöckner,
1111 The SILVA ribosomal RNA gene database project: Improved data processing and web-
1112 based tools. *Nucleic Acids Research* **41**, D590 (2013).

1113 68. E. S. Wright, Using DECIPHER v2.0 to analyze big biological sequence data in R. *R*
1114 *Journal* **8**, 352–359 (2016).

1115 69. J. Oksanen, G. L. Simpson, F. G. Blanchet, R. Kindt, P. Legendre, P. R. Minchin, R. B.
1116 O'Hara, P. Solymos, M. H. H. Stevens, E. Szoecs, H. Wagner, M. Barbour, M. Bedward,
1117 B. Bolker, D. Borcard, G. Carvalho, M. Chirico, M. D. Caceres, S. Durand, H. B. A.
1118 Evangelista, R. FitzJohn, M. Friendly, B. Furneaux, G. Hannigan, M. O. Hill, L. Lahti, D.
1119 McGlinn, M.-H. Ouellette, E. R. Cunha, T. Smith, A. Stier, C. J. F. T. Braak, J. Weedon,
1120 vegan: Community Ecology Package, version 2.6-6.1 (2024); https://cran.r-
1121 project.org/web/packages/vegan/index.html.

1122 70. S. Weiss, Z. Z. Xu, S. Peddada, A. Amir, K. Bittinger, A. Gonzalez, C. Lozupone, J. R.
1123 Zaneveld, Y. Vázquez-Baeza, A. Birmingham, E. R. Hyde, R. Knight, Normalization and

1124 microbial differential abundance strategies depend upon data characteristics.
1125 *Microbiome* **5**, 1–18 (2017).

1126 71. E. Montassier, G. A. Al-Ghalith, B. Hillmann, K. Viskocil, A. J. Kabage, C. E. McKinlay, M.
1127 J. Sadowsky, A. Khoruts, D. Knights, CLOUD: A non-parametric detection test for
1128 microbiome outliers. *Microbiome* **6**, 1–10 (2018).

1129 72. P. J. McMurdie, S. Holmes, phyloseq: an R package for reproducible interactive analysis
1130 and graphics of microbiome census data. *PLoS One* **8**, e61217 (2013).

1131 73. A. Dobin, C. A. Davis, F. Schlesinger, J. Drenkow, C. Zaleski, S. Jha, P. Batut, M. Chaisson,
1132 T. R. Gingeras, STAR: ultrafast universal RNA-seq aligner. *Bioinformatics* **29**, 15–21
1133 (2013).

1134 74. A. Rau, C. Maugis-Rabusseau, Transformation and model choice for RNA-seq co-
1135 expression analysis. *Briefings in Bioinformatics* **19**, 425–436 (2018).

1136 75. J. Abramson, J. Adler, J. Dunger, R. Evans, T. Green, A. Pritzel, O. Ronneberger, L.
1137 Willmore, A. J. Ballard, J. Bambrick, S. W. Bodenstein, D. A. Evans, C.-C. Hung, M.
1138 O'Neill, D. Reiman, K. Tunyasuvunakool, Z. Wu, A. Žemgulytė, E. Arvaniti, C. Beattie, O.
1139 Bertolli, A. Bridgland, A. Cherepanov, M. Congreve, A. I. Cowen-Rivers, A. Cowie, M.
1140 Figurnov, F. B. Fuchs, H. Gladman, R. Jain, Y. A. Khan, C. M. R. Low, K. Perlin, A.
1141 Potapenko, P. Savy, S. Singh, A. Stecula, A. Thillaisundaram, C. Tong, S. Yakneen, E. D.
1142 Zhong, M. Zielinski, A. Žídek, V. Bapst, P. Kohli, M. Jaderberg, D. Hassabis, J. M. Jumper,
1143 Accurate structure prediction of biomolecular interactions with AlphaFold 3. *Nature*
1144 **630**, 493–500 (2024).

1145